Actin networks modulate heterogenous NF-κB dynamics in response to TNFα

Francesca Butera[1,3*], Julia E. Sero[2], Lucas G. Dent[1], Chris Bakal[1*]

[1]Chester Beatty Laboratories, Division of Cancer Biology, Institute of Cancer Research, 237 Fulham Road, London, SW3 6JB, UK

[2]Biology and Biochemistry Department, Bath University, Claverton Down, BA2 7AY, UK

[3]Lead contact

*Correspondence: francesca.butera@icr.ac.uk and chris.bakal@icr.ac.uk

Abstract

The canonical NF-κB transcription factor RELA is a master regulator of immune and stress responses and is upregulated in PDAC tumours. Here, we characterised previously unknown endogenous RELA-GFP dynamics in PDAC cell lines by live single cell imaging, which revealed rapid, sustained and non-oscillatory nuclear RELA following TNFα stimulation. Using Bayesian analysis of single cell datasets with variation in nuclear RELA, we computationally predicted that RELA heterogeneity in PDAC cell lines is dependent on F-actin dynamics. By RNA-seq, we identified the actin regulators NUAK2 and ARHGAP31 as transcriptionally regulated by RELA. In turn, *NUAK2* or *ARHGAP31* siRNA depletion downregulates TNFα-stimulated RELA nuclear localisation in PDAC cells, establishing a novel negative feedback loop regulating RELA activation by TNFα. We identify an additional actin-independent feedback loop involving RELB, which suppresses TNFα-mediated RELA nuclear localisation following RELA mediated upregulation of RELB. Taken together, we provide computational and experimental support for interdependence between the F-actin network and RELA translocation dynamics in PDAC.

Introduction

The NF-κB transcription factor RELA is an essential mediator of the inflammatory and immune responses in all mammals (Hayden et al., 2006) and is central to the canonical NF-κB signalling pathway (Ghosh et al., 1998). As a transcription factor, RELA activation is controlled in large part through its localisation. Inactive RELA is sequestered in the cytoplasm by IκB proteins and IκB degradation by upstream cues, such as the potent inflammatory cytokine Tumour Necrosis Factor α (TNFα), enables RELA translocation to the nucleus where RELA regulates gene expression (DiDonato et al., 1997; Zandi et al., 1997).

Live imaging experiments of fluorescently labelled RELA and electrophoretic mobility shift assays have shown that RELA oscillates between the nucleus and cytoplasm in response to TNFα (Hoffmann et al., 2002; Nelson et al., 2004; Sung et al., 2009; Tay et al., 2010; Sero et al., 2015; Zambrano et al., 2016). Oscillations are driven by a negative feedback loop between RELA and particular IκB isoforms, since the genes encoding IκB proteins are RELA transcriptional targets (Brown et al., 1993; Scott et al., 1993; Sun et al., 1993; Hoffmann et al., 2002). The pattern of RELA translocation has been shown to dictate the specificity and timing of RELA target gene expression, including the genes encoding IκBα, IκBε and the chemokine RANTES (Ashall et al., 2009; Zambrano et al., 2016; Lane et al., 2017). However, most studies characterising RELA translocation dynamics following stimulation use hyperphysiological TNFα doses (e.g. 10 ng/ml) and exogenous RELA reporters.

Previously, we showed that cell shape is a regulator of RELA dynamics in breast cancer cell lines and that breast cancer cells with mesenchymal cell shape (protrusive with low cell-cell contacts) have higher RELA nuclear translocation (Sero et al., 2015). We also identified that RELA activity, coupled to cell shape, is predictive of breast cancer progression (Sailem and Bakal, 2017). Although the mechanistic basis for how cell shape regulates RELA remains poorly understood, studies have shown that chemically inhibiting actin or tubulin dynamics

can increase RELA binding to DNA and RELA-dependent gene expression (Rosette and Karin, 1995; Bourgarel-Rey et al., 2001; Németh et al., 2004).

Despite frequent upregulation of both TNFα and RELA in PDAC tumours (Weichert et al., 2007; Zhao et al., 2016), the dynamics and regulation of single cell RELA translocation, as well as RELA transcriptional output, are poorly understood for PDAC cells. Here, we used CRISPR-CAS9 to tag RELA with GFP in the human cell lines MIA PaCa2 and PANC1 and identified rapid, non-oscillatory and heterogenous RELA dynamics by live imaging. To explore potential cytoskeletal or cell shape regulation of RELA in PDAC, we constructed Bayesian models using single cell datasets from TNFα-stimulated PDAC cells with variation in RELA, actin and tubulin measurements for hypothesis generation: one dataset with five PDAC cell lines and another with diverse small-molecules targeting cytoskeletal components. Notably, nuclear RELA was statistically predicted to be dependent on actin features across Bayesian models. Finally, we used RNA-seq to identify genes with distinct patterns of expression based on dependence on TNFα dose and RELA activation. Using live imaging with knockdown of selected targets, our results uncover novel mechanisms regulating inflammation-associated RELA dynamics in PDAC, including negative feedback loops between RELA and the actin modulators NUAK2 and ARHGAP31, and between RELA and the non-canonical NF-κB factor RELB.

67 # Results

68 **Single cell endogenous RELA responses to TNFα are non-oscillatory and sustained**
69 **in PDAC cells**

70 To study PDAC biology, we used the frequently studied human PDAC cell lines MIA PaCa2
71 and PANC1, which harbour key genomic alterations in PDAC, including KRAS and p53
72 mutations and homozygous deletions in CDKN2A/p16 (Deer et al., 2010). In addition, MIA
73 PaCa2 and PANC1 cells are epithelial in origin but have distinct cell morphologies and are
74 therefore useful for analysis of cell shape interaction with RELA. To study dynamic RELA
75 localisation changes, we used CRISPR-CAS9 gene editing to fluorescently tag endogenous
76 RELA at the C-terminus with eGFP (abbreviated as RELA-GFP) (Figure 1A and 1B). The C-
77 terminus was selected to avoid interference with the N-terminal Rel homology domain, which
78 contains the transactivation, nuclear import and DNA-binding domains (Kieran et al., 1990;
79 Nolan et al., 1991). GFP+ clones were selected using FACS, single cell sorted and expanded
80 into monoclonal cell lines. We also introduced mScarlet-I to the C-terminus of PCNA
81 (Proliferating Cell Nuclear Antigen; abbreviated as PCNA-Scarlet) – a processivity factor for
82 DNA polymerase δ that functions during replication – which served as a nuclear marker for
83 segmentation and as a cell cycle marker (Kurki et al., 1986; Barr et al., 2017) (Figure 1A and
84 1B).

85 To observe live RELA translocation dynamics in response to inflammatory stimuli, we used
86 timelapse confocal microscopy with automated image analysis to track changes in RELA-
87 GFP localisation on a single cell level in response to TNFα (0.01, 0.1 and 10 ng/ml), from -
88 120 min to +600 min relative to TNFα addition. 0.01 ng/ml TNFα is a physiological dose
89 relevant to healthy and malignant tissue, while 0.1 ng/ml TNFα is detected in highly
90 inflammatory PDAC microenvironments (Zhao et al., 2016). 10 ng/ml TNFα was used in
91 several studies assaying RELA translocation (Hoffmann et al., 2002; Tay et al., 2010; Sero

et al., 2015) and is included for comparison, but is substantially above physiological levels (Zhao et al., 2016).

Broadly, we observed a lack of oscillatory nuclear RELA dynamics in PDAC cells, in addition to general maintenance of nuclear RELA across the 10 hr imaging period. MIA PaCa2 cells responded with higher nuclear RELA compared to PANC1 cells at each TNFα dose (Figure 1C). The highest nuclear RELA measurement attained on the single cell level, referred to as 'peak RELA', was statistically significantly different between 0.01 and 0.1 ng/ml for MIA PaCa2 but not for PANC1 cells, suggesting that MIA PaCa2 cells are more sensitive to TNFα in terms of RELA activation (Figure 1D). 10 ng/ml TNFα elicited a significantly higher nuclear RELA localisation amplitude in both cell lines compared to lower TNFα doses (0.01 and 0.1 ng/ml). In contrast, TNFα dose did not affect the time to peak RELA in either cell line (Figure 1E), although the time to peak RELA was highly heterogenous on the single cell level within each TNFα dose, suggesting that the time to peak RELA is controlled by multiple cell intrinsic factors.

We also compared RELA measurements within each single cell track to assess the stability of nuclear RELA levels (Figure 1F). In MIA PaCa2 cells, there is a high correlation between nuclear RELA at latter timepoints (180, 300 or 600 min) compared to an early timepoint (60 min) following TNFα addition. PANC1 cells have high correlation between nuclear RELA measurements at 60 min RELA and 180 min, while there is weak correlation between RELA levels at 60 min and 600 min. Thus, in MIA PaCa2, but not PANC1, RELA translocation at 60 min is largely predictive of long-term response to TNFα.

Overall, our data show that RELA nuclear translocation occurs rapidly, and in a non-oscillatory fashion in both MIA PaCa2 and PANC1 cells in response to TNFα. In MIA PaCa2 cells, RELA translocation is largely sustained for hours, while damped in PANC1 cells.

116 **RELA translocation responses to TNFα are cell cycle independent**

117 To identify whether cell cycle progression contributes to heterogeneity in RELA responses
118 to TNFα in PDAC cells, we categorised each tracked cell by cell cycle stage at the time of
119 TNFα addition, using changes in the appearance and intensity of endogenous PCNA-Scarlet
120 to mark cell cycle transitions (Figure 1 - Supplement 1A). For each cell, we calculated the
121 amplitude and timing of peak nuclear RELA, in addition to the mean nuclear RELA intensity
122 across all timepoints. Largely, there were no differences between cells by cell cycle stage in
123 terms of peak RELA measurements (amplitude or timing) in MIA PaCa2 and PANC1 cells
124 (Figure 1 - Supplement 1C, D). However, we identified statistically significant higher (whole
125 track) mean nuclear RELA in G2 cells in the PANC1 cell line alone (Figure 1 - Supplement
126 1E).

127 **TNFα-mediated RELA heterogeneity in PDAC cells is predicted to be dependent on**
128 **actin dynamics**

129 Because the same TNFα concentration can lead to variable responses, we proposed that
130 there are cell-intrinsic mechanisms that dictate the extent of RELA translocation in PDAC
131 cells. Having previously identified relationships between cell shape and RELA localisation in
132 breast cells (Sero et al., 2015), we hypothesised that differences in actin and tubulin
133 organisation, which regulate cell shape (Machesky and Hall, 1997, Desai and Mitchison,
134 1997), may explain differences in RELA dynamics. To test this, we expanded our dataset to
135 include immunofluorescence images of the human immortalised PDAC cell lines MIA PaCa2,
136 PANC1, Capan1, SW1990 and PANC05.04. We treated cells with TNFα (1 hr), or with
137 solvent control, and stained for DNA, RELA, F-actin and α-tubulin (Figure 2 - Supplement
138 1A). We used automated image analysis to segment cell regions and measured 35
139 geometric, cytoskeletal and Hoechst features, as well as nuclear RELA, in approximately
140 130,000 cells. The 35 cell features were then reduced by hierarchical clustering to a subset
141 of ten features (Figure 2 - Supplement 1B). Selected features include classical

142 measurements of cell shape (‘Cell Area’, ‘Cell Roundness’ and ‘Nucleus Roundness’), mean
143 measurements and texture analysis of actin and tubulin intensity in the cytoplasm, and the
144 ratio of ‘Actin filament area’ to ’Cell area’ which assays actin stress fibre abundance (Figure
145 2 - Supplement 1C).

146 We used principal component analysis (PCA) to assess the morphological diversity of the
147 five PDAC cell lines using normalised data for cells under control conditions (Figure 2 -
148 Supplement 2). PCA largely clustered data by cell line, indicating distinct cell morphology
149 and cytoskeletal organisation between PDAC cell lines. PCA also validated that the reduced
150 cell feature set is sufficient to capture the morphological heterogeneity in the PDAC lines.
151 Notably, MIA PaCa2 cells scored low on several cell features due to these cells having
152 particularly small cell area, distorted nuclei (low nucleus roundness) and low actin
153 abundance. Moreover, in MIA Paca2 cells, actin is localised in areas of the cytoplasm distal
154 to the membrane. In contrast, PANC1 cells have a notably high cell and nucleus roundness,
155 as well as high membrane/cyt actin, indicating that actin in PANC1 cells is localised
156 predominantly at the cortex.

157 Distributions of nuclear RELA in the five PDAC cell lines by immunofluorescence revealed
158 highly heterogeneous RELA responses within and across the PDAC cell lines (Figure 2A).
159 To identify features that predict RELA localisation differences, we collated and incorporated
160 normalised single cell measurements across all PDAC cell lines and TNFα treatments into
161 Bayesian networks, harnessing the observed variation in RELA (Figure 2B). Bayesian
162 network models apply statistical inference to heterogeneous experimental data to predict the
163 conditional dependence of components on each other. Bayesian network models appear as
164 influence diagrams consisting of nodes, each representing a measured feature, and arcs
165 that depict predicted dependencies between the nodes. These dependencies represent
166 linear and non-linear relationships, direct and indirect interactions, and illustrate multiple
167 interacting nodes simultaneously (Sachs et al., 2005). We employed a hybrid class of

168 Bayesian algorithm (‘rsmax2’) that generates models with unidirectional arcs using a
169 combination of constraint-based and score-based approaches (Scutari et al., 2018).

170 In order to provide the greatest heterogeneity in nuclear RELA and cytoskeletal/cell shape
171 features for Bayesian model generation, we collated data from all five PDAC lines and TNFα
172 doses (0, 0.01, 0.1 and 10 ng/ml), shown in Figure 2C. This model indicated that nuclear
173 RELA measurements are correlated to and predicted to be dependent on cytoplasmic actin
174 and tubulin intensity, suggesting that cytoskeletal dynamics influence heterogeneity in
175 nuclear RELA translocation with TNFα. Nuclear RELA is also predicted to be dependent on
176 cell area, although with a lower strength of the probabilistic relationship compared to
177 actin/tubulin, while nucleus roundness is predicted to be dependent on nuclear RELA.
178 Interestingly, both actin texture and the ratio of membrane to cytoplasm actin are also
179 predicted to be dependent on RELA, suggesting that RELA and actin dynamics are
180 interdependent. Altogether, our data suggest that the influence of cell shape on RELA
181 translocation we have previously described in breast cancer cells (Sero et al., 2015; Sailem
182 and Bakal, 2017) is likely mediated through cytoskeletal changes.

183 To understand how inter-line differences in cytoskeletal organisation may influence RELA
184 translocation dynamics, we additionally generated Bayesian network models by subsetting
185 data by cell line and TNFα concentration. We summarised dependencies involving nuclear
186 RELA in Figure 2D. In contrast to our prior findings using Bayesian modelling of RELA and
187 cell shape with breast cancer cells in the absence of cytoskeletal measurements (Sero et al.,
188 2015; Sailem and Bakal, 2017), here we found a general lack of dependence of nuclear
189 RELA on cell shape features, but identified strong and consistent dependencies of nuclear
190 RELA on cytoplasm actin and tubulin, as well as actin texture, in several PDAC cell lines and
191 TNFα doses (Figure 2D). These data computationally predict that actin and tubulin
192 abundance and actin distribution within the cell influence RELA nuclear translocation.

193 When using datasets of sufficient size, deriving Bayesian models based on largely stochastic
194 and relatively small fluctuations in variables can provide insight into the influence of
195 cytoskeletal components, shape, and RELA on each other (Figure 2C). But molecular
196 interventions provide a means to further drive ordering of connections by identifying regions
197 in state where normally correlated variables become conditionally independent (Pe'er et al.,
198 2001; Sachs et al., 2005). Consequently, we created an additional dataset where cells were
199 imaged following perturbations of tubulin, actin, myosin, or focal adhesion (FA) dynamics
200 (Figure 2E). Such perturbations are intended to alter the value of variables/features (i.e.
201 measures of actin organisation) beyond those observed in normal populations.

202 For example, CK666 inhibits the ARP2/3 complex – a key mediator of actin filament
203 nucleation and branching (Mullins et al., 1998), while SMIFH2 inhibits formins (Rizvi et al.,
204 2009), which promote actin nucleation and elongation of pre-existing filaments to produce
205 long straight filaments (Pruyne et al., 2002). H1152 targets Rho-kinase (ROCK), preventing
206 ROCK phosphorylation of myosin light chain that normally promotes actin-binding and
207 consequently contractility, while blebbistatin blocks myosin II ATPase and subsequently
208 interferes with actin contractility (Sasaki et al., 2002; Kovács et al., 2004). Tubulin-targeting
209 drugs are commonly used in cancer chemotherapy and either prevent MT assembly
210 (vinblastine and nocodazole), limit MT formation and cause MT depolymerisation
211 (demecolcine), or stabilise MTs and prevent disassembly (paclitaxel) (Spencer and Faulds,
212 1994; Vasquez et al., 1997; Gigant et al., 2005; Tangutur et al., 2017). We ascertained
213 optimal doses by treating MIA PaCa2 cells with dose ranges for 24 hr, or 3 hr for SMIFH2
214 (Figure 2 - Supplement 3).

215 We generated a single cell dataset for use in Bayesian modelling by treating MIA PaCa2 and
216 PANC1 cells with selected drug doses for 2 hr then simultaneously with TNFα (0, 0.01, 0.1
217 and 10 ng/ml) for 1 hr and input these data into the same Bayesian algorithm as above
218 (rsmax2) (Figure 2F). Interestingly, the Bayesian network following perturbations revealed
219 that 5/6 of the variables observed to correlate with RELA (whether they influenced RELA or

were influenced by RELA) in untreated cells were independent of RELA in the drug-treated network. Only 'Cytoplasmic Actin Mean' remained as a influencing variable following drug-treatment, suggesting that actin abundance is a key regulator of RELA nuclear localisation. While other variables (i.e. Tubulin and cell shape) can indirectly influence RELA, they do so via regulating actin network organisation.

TNFα dose and duration determine profiles of RELA-dependent gene expression in PDAC cells

As RELA is known to be involved in feedback loops with transcriptional targets, with the best studied example being IκBα, we sought to identify what the transcriptional targets of RELA are in PDAC and which influence RELA in actin dependent and independent ways.

To this end, we carried out RNA-seq analysis of PDAC cells at an early (1 hr) and late (5 hr) timepoint with varying TNFα doses (0.01, 0.1 or 10 ng/ml TNFα) using MIA PaCa2 and PANC1 cells. TNFα treatments were in the presence or absence of dox-induction of IκB super repressor (IκB-SR) to determine which genes require RELA nuclear translocation. 236 genes were differentially expressed in high TNFα (0.1 or 10 ng/ml) versus basal conditions, with the majority of genes (186) upregulated by TNFα (Figure 3A and 3B).

To identify patterns of gene expression across TNFα doses and durations, the 236 TNFα-regulated genes were organised by hierarchical clustering into seven clusters, each with distinct expression dynamics or dependence on RELA (Figure 3C and 3D). Cluster 3 shows genes with clear dependence on RELA activation in both MIA PaCa2 and PANC1 cells and has genes significantly upregulated by TNFα in a dose-dependent manner. Moreover, Cluster 3 genes are more highly upregulated by TNFα in MIA PaCa2 compared to PANC1 cells, which is consistent with the RELA dynamics observed by live imaging whereby 0.1 ng/ml is sufficient to increase RELA nuclear localisation in MIA PaCa2 but not PANC1 cells (Figure 1D). Cluster 3 genes also have higher RELA expression at 5 hr TNFα compared to 1 hr TNFα in both cell lines, indicating that they are associated with prolonged RELA

246 activation. As expected from the RELA and TNFα dose dependent properties of this cluster,
247 known RELA targets such as RELB, NFKB2 and BIRC3 are present (Lombardi et al., 1995;
248 Bren et al., 2001; Frasor et al., 2009), and also has the immune ligands CD70 and CD83.
249 Notably, Cluster 3 contains Rho GTPase activating protein 31 (ARHGAP31) and NUAK
250 family kinase 2 (NUAK2), which are involved in the regulation of actin (Tcherkezian et al.,
251 2006; Vallenius et al., 2011).

252 Two clusters of TNFα-regulated genes in PDAC cells are downregulated by TNFα (Figure
253 3C and 3D) in a dose-independent manner: Cluster 1 and Cluster 2. Cluster 1 consists of
254 long non-coding RNAs (lncRNAs) and are further downregulated by IκB-SR in the MIA
255 PaCa2 cell line only, suggesting that RELA and TNFα have antagonistic effects on the
256 expression of these lncRNAs. In contrast, Cluster 2 genes are entirely independent of RELA.

257 The remaining clusters (Figure 3C and 3D) contain genes upregulated by TNFα. Cluster 4
258 genes are similar to Cluster 3 in that their expression is higher at 5 hr versus 1 hr, but Cluster
259 4 genes have more moderate upregulation by TNFα. Moreover, Cluster 4 genes appear only
260 to be RELA-dependent with 5 hr TNFα. Clusters 5 and 7 are upregulated by TNFα in a dose
261 independent manner. Finally, genes in Cluster 6 are dependent on TNFα dose but not
262 duration.

263 Overall, we identified gene expression patterns linked to TNFα dose and duration, as well
264 as variable dependence on RELA, suggesting that TNFα/RELA dynamics determine
265 transcriptional output in PDAC cells.

266 **RELA modulates the expression of and physically interacts with non-canonical NF-κB**
267 **and the IκB proteins in PDAC cells**

268 Having observed sustained and non-oscillatory nuclear RELA with TNFα (Figure 1), we
269 decided to consider in more detail how the expression of NF-κB transcription factors and IκB
270 family proteins are affected by TNFα dose and RELA inactivation by IκB-SR in PDAC cells,

271 given that IκB proteins are known regulators of RELA across cell types (Baeuerle and
272 Baltimore, 1988).

273 RNA-seq in MIA PaCa2 and PANC1 cells revealed that expression of *RELA* itself did not
274 significantly scale with TNFα dose, while *RELB* and the transcriptionally incompetent NF-κB
275 proteins *NFKB1* and *NFKB2* showed increasing expression with increasing TNFα (Left graph
276 in Figure 3 - Supplement 1A). TNFα addition significantly altered the expression of a subset
277 of IκB protein-encoding genes, which display distinct expression dynamics: *NFKBIA* (Figure
278 3: Cluster 5), *NFKBIB* (Figure 3: Cluster 4), *NFKBIE* (Figure 3: Cluster 3), *NFKBID* (Figure
279 3: Cluster 6) and *NFKBIZ* (Figure 3: Cluster 6). Of these, *NFKBIA* has the highest absolute
280 RNA expression in MIA PaCa2 cells and *NFKBIB* has the highest abundance in PANC1
281 cells, while *NFKBID* and *NFKBIZ* have the lowest RNA expression in both cell lines (right
282 graph in Figure 3 - Supplement 1A).

283 T-test comparison with multiple test correction of RNA expression in TNFα-treated cells
284 revealed that *RELB* and *REL* have significantly reduced expression with IκB-SR presence
285 versus absence in both MIA PaCa2 and PANC1 cells, while *NFKB2* is only affected by IκB-
286 SR induction in PANC1 cells (Figure 3 - Supplement 1A'). Furthermore, expression of the
287 canonical RELA binding partner *NFKB1* is unaffected by RELA-inactivation by IκB-SR in both
288 cell lines. Similarly, expression of the IκB family protein-encoding genes *NFKBIA* and
289 *NFKBIB* were not significantly impacted by RELA inactivation in either cell line, while *NFKBIE*
290 expression was reduced with IκB-SR in PANC1. Therefore, of the core NF-κB signalling
291 components, *RELB*, *REL* and *NFKBIE* expression appear to be dependent on TNFα-
292 stimulated RELA nuclear translocation in PDAC cells.

293 We also considered how expression of NF-κB and IκB genes are affected by the treatment
294 duration of TNFα (Figure 3 - Supplement 1A''), combining data from 0.1 ng/ml and 10ng/ml
295 TNFα. In both MIA PaCa2 and PANC1 cells, *RELB* expression was significantly higher with

296 5 hr compared to 1 hr TNFα, which was also the case for *NFKB2* and *NFKBIE* in the PANC1
297 cell line alone.

298 Lastly, we checked which NF-κB/IκB proteins interact with RELA in PDAC cells. GFP-Trap
299 followed by mass spectrometry with MIA PaCa2 cells expressing endogenously tagged
300 RELA-GFP pulled down six NF-κB/IκB proteins (Figure 3 - Supplement 1B). IκBα/NFKBIA,
301 IκBβ/NFKBIB and IκBε/NFKBIE were pulled down at lower abundance with increasing TNFα
302 dose, in line with the well-studied degradation of IκB proteins downstream of TNFα
303 stimulation (Chen et al., 1995). Interestingly, the NF-κB protein REL also had reduced
304 interaction with RELA with TNFα. In contrast, NFKB1 and NFKB2 showed increased
305 interaction with RELA with TNFα. RELA therefore appears to form NF-κB heterodimers with
306 REL, NFKB1 and NFKB2 in PDAC cells.

307 **The NF-κB signalling components RELB and IκBβ and the actin modulators**
308 **ARHGAP31 and NUAK2 suppress TNFα-stimulated RELA nuclear localisation in**
309 **PDAC cells**

310 To test for potential feedback loops regulating RELA in PDAC, we evaluated the effect of
311 siRNA knockdown of TNFα-regulated genes on TNFα-stimulated RELA dynamics. We
312 targeted the genes encoding the known RELA inhibitors IκBα, IκBβ and IκBε, which were
313 pulled down with RELA-GFP by GFP-Trap, and the non-canonical NF-κB transcription
314 factors RELB and NFKB2. In addition, we tested knockdown of the Cluster 3 (from Figure 3)
315 genes *NUAK2* and *ARHGAP31*, which are known actin modulators (Tcherkezian et al., 2006;
316 Vallenius et al., 2011). MIA PaCa2 and PANC1 cells were transfected with siRNAs for 48 hr
317 then live imaged for 2 hr prior to until 12 hr following addition of 10 ng/ml TNFα or solvent
318 control (Figure 4A-D). We used non-targeting (NT) siRNA as a negative control for
319 comparison and verified transfection efficacy using RELA siRNA, which abrogated the
320 nuclear RELA signal (Figure 4A).

321 To identify whether siRNAs affected the early/peak RELA and sustained RELA response to
322 TNFα, we calculated the fold change of mean nuclear RELA with each siRNA to NT siRNA
323 at 1 hr or 12 hr TNFα stimulation, and compared fold changes using t-test with multiple
324 comparison correction (Figure 4B and 4C). Considering TNFα/NF-κB pathway components,
325 we found that several siRNAs enhanced nuclear RELA in PANC1 but not in MIA PaCa2 in
326 basal conditions, including *NFKBIA*, *NFKBIB*, *RELB* and *ARHGAP31*, suggesting that RELA
327 activation is actively and constitutively suppressed by several mechanisms in PANC1 cells.

328 Focusing on the early RELA response (1 hr) to TNFα, we found that *NFKBIE* and *NFKB2*
329 depletion reduced nuclear RELA in PANC1 in control conditions, suggesting that these
330 TNFα/NF-κB signalling components enhance nuclear RELA in basal conditions. Meanwhile,
331 depletion of *NFKBIA*, *NFKBIE*, and *RELB* significantly increased nuclear RELA in basal and
332 TNFα conditions in PANC1.

333 In terms of the RELA response to 12 hr post-TNFα, we observed more pronounced effects
334 with TNFα in MIA PaCa2 compared to with 1 hr post-TNFα. In particular, depletion of *RELB*
335 and *NFKBIB*, but not *NFKBIA* or *NFKBIE*, significantly enhanced nuclear RELA. In PANC1
336 cells, *NFKBIE* and *NUAK2* siRNA depletion reduced nuclear RELA in basal conditions. In
337 contrast, none of these gene depletions affected TNFα-regulated nuclear RELA with PANC1,
338 which was significantly increased by depletion of *NFKBIA* and *NFKBIB*.

339 Overall, *RELB* and *NFKBIB* suppressed nuclear RELA in multiple contexts and may
340 therefore be key regulators of RELA dynamics with TNFα in PDAC. However, despite
341 implication of IκBβ and IκBε in the suppression of RELA oscillations (Hoffmann et al., 2002),
342 we did not observe RELA oscillations with *NFKBIB* and *NFKBIE* depletion in PDAC cells,
343 suggesting that the lack of RELA oscillations in PDAC cells may be more related to IκBα or
344 via independent positive feedback mechanisms.

345 We then focused on the effect of siRNA knockdown of the putative actin regulators and
346 TNFα/RELA-dependent genes *ARHGAP31* and *NUAK2* on early (1 hr post-TNFα) and late

347 (12 hr post-TNFα) nuclear RELA in MIA PaCa2 and PANC1 cells, in order to explore the
348 dependence of RELA on actin dynamics computationally predicted by Bayesian modelling
349 (Figure 2). Strikingly, *ARHGAP31* depletion significantly increased the early (1 hr) response
350 of PANC1 cells to TNFα and the late (5 hr) response of MIA PaCa2 to TNFα, while NUAK2
351 depletion increased nuclear RELA with TNFα in MIA PaCa2 cells (Figure 4B and 4C). Thus,
352 *NUAK2*/*ARHGAP31* expression impacts TNFα-mediated RELA dynamics in PDAC cells.

353 We additionally checked whether depletion of *ARHGAP31* or *NUAK2* altered actin and cell
354 shape using Phalloidin staining with each siRNA (Figure 4 - Supplement 1). MIA PaCa2 and
355 PANC1 cells in the presence of *ARHGAP31* siRNA showed flatter morphology and reduction
356 of stress fibre abundance, while *NUAK2* siRNA visibly increased actin abundance and the
357 presence of lamellipodia in both cell lines.

358 Therefore, we identified RELA targets (*ARHGAP31*/*NUAK2*) involved in actin modulation
359 that additionally downregulate nuclear RELA with TNFα, providing a potential mechanism
360 that may mediate the relationship between actin and RELA.

361 ## Discussion

362 To characterise previously unknown single cell RELA dynamics in PDAC cells, we used
363 CRISPR-CAS9 genome editing to tag RELA endogenously with GFP in the human PDAC
364 cell lines MIA PaCa2 and PANC1. Using live imaging and automated image analysis, we
365 characterised RELA responses to the cytokine TNFα, which is upregulated with PDAC
366 progression (Zhao et al., 2016). Strikingly, PDAC cells show atypical RELA dynamics
367 compared to reports in cells from other tissues (Ashall et al., 2009; Tay et al., 2010; Sero et
368 al., 2015), as we observed that PDAC cells maintain prolonged nuclear RELA localisation
369 and RELA responses are cell cycle independent. However, we identified that a key difference
370 between MIA PaCa2 and PANC1 cells is that MIA PaCa2 cells respond with higher and
371 sustained RELA nuclear localisation compared to PANC1 cells, while PANC1 cells have a
372 damped RELA response over time. Similar to other cell lines (Ashall et al., 2009; Tay et al.,
373 2010; Sero et al., 2015), we found that RELA nuclear translocation in PDAC cells occurs
374 immediately following TNFα addition and peak nuclear RELA localisation occurs around 1 hr
375 post-TNFα.

376 The distinct RELA dynamics between PDAC with reports from other tissues may be
377 attributed to the use of knock-in RELA-GFP in this study, since most studies used exogenous
378 RELA fusion constructs (Ashall et al., 2009; Tay et al., 2010; Sero et al., 2015). As RELA
379 upregulates several genes involved in positive and negative feedback (Collart et al., 1990;
380 Libermann and Baltimore, 1990; Brown et al., 1993; Scott et al., 1993; Sun et al., 1993),
381 which we observed in the present study using RNA-seq, RELA overexpression could
382 interfere with its intrinsic dynamics. Nonetheless, other studies that have tagged RELA
383 endogenously did detect oscillations, including MEFs (Sung et al., 2009; Zambrano et al.,
384 2016) and MCF7 breast cancer cells (Stewart-Ornstein and Lahav, 2016).

385 The high sensitivity of PDAC cells to TNFα and lack of oscillations suggest that PDAC cells
386 may suppress negative feedback imposed by IκBα, as Hoffman et al. (2002) demonstrated

387 that oscillations in NF-κB DNA binding are due to negative feedback with IκBα, which is
388 encoded by a gene (*NFKBIA*) upregulated by NF-κB factors. Hoffman et al. also identified
389 that cells with high IκBβ and IκBε expression, or absence of IκBα, lose oscillations stimulated
390 by TNFα. These findings motivated our inspection into RELA interaction with IκB proteins
391 and upregulation of IκB genes by TNFα in PDAC cells. Using co-immunoprecipitation of
392 RELA with MIA PaCa2 cells, we found that RELA binds to IκBα, IκBβ and IκBε and binding
393 to each is suppressed in high TNFα concentrations. However, contrary to our expectations
394 based on the findings by Hoffmann et al., we did not observe RELA oscillations with *NFKBIB*
395 or *NFKBIE* depletion in MIA PaCa2 or PANC1 cells, suggesting that the lack of RELA
396 oscillations in these cell lines may be due to enhanced positive feedback and/or insufficient
397 *NFKBIA* expression.

398 We used Bayesian modelling as an unbiased and high dimensional approach to determine
399 whether descriptors of cell shape and the cytoskeleton correlate with the observed
400 heterogeneity in RELA localisation, having previously used Bayesian modelling to show that
401 RELA localisation in breast cells is strongly dependent on neighbour contact, cell area, and
402 protrusiveness in the presence and absence of TNFα (Sero et al., 2015). In the present
403 study, we extended the analysis to include measurements of actin and tubulin organisation.
404 Since Bayesian modelling relies on heterogeneity in measurements to make predictions, we
405 used a dataset with five PDAC cell lines with high intra and inter-line variability in RELA, as
406 well as distinct cell shape and cytoskeleton between the cell lines. We independently ran
407 Bayesian modelling with a dataset of cells with perturbation of the cytoskeleton using small
408 molecules, based on the seminal study by Sachs et al. (2005) that used Bayesian inference
409 to derive cell signalling networks. Consistently among our models, differences in cytoplasmic
410 actin intensity, as well as measures of actin localisation (cortical versus cytoplasmic actin),
411 were predictive of differences in nuclear RELA between single PDAC cells.

412 To identify potential regulatory loops involving RELA in PDAC, we used RNA-seq analysis
413 with MIA PaCa2 and PANC1 cells treated with varying TNFα doses +/- IκB-SR. We identified

414 236 genes significantly regulated by TNFα, which may be viewed as candidates for targeting
415 NF-κB signalling or output in PDAC. Identifying novel targets for PDAC is important as the
416 5-year survival rate of non-resected PDAC patients has remained unchanged from 1975 to
417 2011 (Bengtsson et al., 2020). Moreover, RELA is hyperactive in 50-70 % of PDAC tumours
418 (Wang et al., 1999; Weichert et al., 2007) and contributes to both cancer progression (Fujioka
419 et al., 2003; Melisi et al., 2009) and resistance to chemotherapy (Bold et al., 2001;
420 Kunnumakkara et al., 2007).

421 Of note, we present the first evidence that *ARHGAP31* is a transcriptional target of TNFα or
422 RELA. Moreover, ARHGAP31 is not previously associated with pancreatic cancer, but has
423 well studied roles in actin modulation, since ARHGAP31 is the human orthologue for the
424 mouse protein CdGAP (mCdc42 GTPase-activating protein) and ARHGAP31 inactivates the
425 GTPases CDC42 and RAC1 (Lamarche-Vane and Hall, 1998; Tcherkezian et al., 2006).
426 CDC42 is involved in the formation of premigratory filopodia in PDAC cells and promotes
427 invasiveness (Razidlo et al., 2018), while RAC1 expression is required for the development
428 of PDAC tumours, in addition to the formation of the ADM and PanN precursors in $KRAS^{G12D}$
429 mouse models (Heid et al., 2011), indicating that RAC1 may play a role in actin remodelling
430 during PDAC initiation.

431 Our results also demonstrate that TNFα upregulates RNA expression of the kinase-encoding
432 gene *NUAK2* (SNARK), while *NUAK2* expression is abrogated in the presence of IκB-SR.
433 Our identification of a feedback loop between RELA nuclear translocation and *NUAK2*
434 expression is analogous to prior findings that NUAK2 increases the activity of the
435 mechanosensitive transcriptional coactivator YAP through stimulation of actin polymerisation
436 and myosin activity (Yuan et al., 2018). A potential source for further study could consider
437 myosin phosphatase target subunit 1 (MYPT1), a substrate for NUAK2 (Yamamoto et al.,
438 2008) that is reported to mediate NUAK2 regulation of actin stress fibres in growing cells
439 (Vallenius et al., 2011). From a therapeutic perspective, NUAK2 may be a promising target
440 to follow-up for potential use in PDAC therapy, as kinases contain an ATP-binding cleft that

441 is a druggable pocket and can contain additional druggable sites distal to the ATP or
442 substrate binding pockets conferring inhibitor specificity (Lamba and Ghosh, 2012).
443 However, NUAK2 is a prognostic marker for PDAC and is associated with a favourable
444 prognosis according to The Human Protein Atlas, which proposes a potential tumour
445 suppressor role for NUAK2 in PDAC, suggesting that enhancing NUAK2 may be a favourable
446 strategy for PDAC. Therefore, our data provide incentive for exploration of a RELA-NUAK2
447 signalling axis in PDAC progression and response to therapy.

Author Contributions

F.B., J.E.S., and C.B. conceived the study. F.B. performed the experiments and image analysis. F.B. and C.B. wrote the manuscript with support and discussion from J.E.S. and L.D..

Acknowledgements

We thank Theodoros I Roumeliotis and Jyoti Choudhary for performing protein mass spectrometry and analysis. We thank Andrea Brundin for assistance with single cell tracking. We gratefully acknowledge funding for this work by Cancer Research UK, awarded to F.B. (S_3567).

Declaration of Interests

The authors declare no competing interests.

459 ## Materials and Methods

460 Further information and requests for resources should be directed to and will be fulfilled by
461 Chris Bakal (chris.bakal@icr.ac.uk).

462 *Cell Lines and Cell Culture*

463 Cell lines were maintained at 37°C and 5% CO2 in Dulbecco's Modified Eagle Medium
464 (DMEM; Gibco) supplemented with 10% heat-inactivated Fetal Bovine Serum (Sigma) and
465 1% Penicillin/Streptomycin (Gibco). MIA PaCa-2, PANC-1, Capan-1, SW-1990, and
466 Panc05.04 were obtained from ATCC.

467 *Generation of cell lines with fluorescently tagged RELA and PCNA by CRISPR-CAS9*

468 RELA and PCNA were tagged endogenously at each C-terminus using CRISPR-CAS9-
469 mediated gene editing in MIA PaCa2 and PANC1 cells. RELA was tagged with enhanced
470 GFP (Zhang et al., 1996) and PCNA was tagged with mScarlet-I (Bindels et al., 2017),
471 abbreviated here as RELA-GFP and PCNA-Scarlet respectively. RELA-GFP was first
472 introduced into wildtype cell lines then PCNA-mScarlet was added to validated RELA-GFP
473 clones.

474 Homology constructs were generated by extracting the region around the stop codon of each
475 gene by PCR. The product was used as a template to amplify the left homology arm (LHA)
476 and right homology arm (RHA) by PCR. PCRs were carried out using High-Fidelity Q5 DNA
477 Polymerase (NEB) according to the manufacturer's protocol. The RHA contains a mutation
478 corresponding to the gRNA protospacer adjacent motif (PAM) to prevent repeat targeting by
479 the Cas9 nuclease. Primers used to amplify the homology arms included overlaps for 1) a
480 DNA cassette encoding a linker protein, the fluorescent protein, and antibiotic resistance
481 (kindly donated by Francis Barr); 2) the pBluescript II SK (-) vector (Agilent) following EcoRV

482 digestion. The final homology construct was generated from the four DNA oligos by Gibson
483 assembly using the NEB Gibson Assembly Master Mix and according to the NEB protocol.

484 gRNA oligos were designed using CRISPR.mit.edu. Forward and reverse oligos were
485 phosphorylated, annealed and ligated into a BbsI-digested pX330 U6 Chimeric hSpCas9
486 plasmid, gifted from Feng Zhang (Cong et al., 2013).

487 Custom oligos were synthesised by Sigma-Aldrich. gRNA oligos were designed using
488 CRISPR.mit.edu.: TGAGTCAGATCAGCTCCTAA (RELA gRNA forward),
489 TTAGGAGCTGATCTGACTCA (RELA gRNA reverse), CGAGGATGAAGAAGGATCTT
490 (PCNA gRNA forward), AAGATCCTTCTTCATCCTCG (PCNA gRNA reverse). The following
491 oligos were used for genomic DNA extraction: TGGGTCAGATGGGGTAAGAG (RELA C-
492 terminus forward), CCAGCTTGGCAACAGATTTA (RELA C-terminus reverse),
493 GCCCTGGAGCCTTGATATTCA (PCNA C-terminus forward),
494 TCTCACTTGTTCCTTGAGCTCA (PCNA C-terminus reverse). The following oligos were
495 used for homology construct generation, using the genomic DNA as a template:
496 ACGGTATCGATAAGCTTGATTGGGTCAGATGGGGTAAGAG (RELA left arm forward),
497 CGCCACCACCGCTCCCACCGGAGCTGATCTGACTCAGCA (RELA left arm reverse),
498 TTCTTGACGAGTTCTTCTGAGGAGGTGACGCCTGCCCTCC (RELA right arm forward),
499 CCGGGCTGCAGGAATTCGATCAAGGAAGTCCCAGACCAAA (RELA right arm reverse),
500 ACGGTATCGATAAGCTTGATGAGTTTGCAGAGCTGAAATTA (PCNA left arm forward),
501 CGCCACCACCGCTCCCACCAGATCCTTCTTCATCCTCGA (PCNA left arm reverse),
502 GTTATGTGTGGGAGGGCTAAGCATTCTTAAAATTCAAGAA (PCNA right arm forward),
503 CCGGGCTGCAGGAATTCGATTCTCACTTGTTCCTTGAGCT (PCNA right arm reverse).

504 Cells were transfected with homology and gRNA constructs using Lipofectamine 2000
505 (ThermoFisher) according to the manufacturer's protocol. Cells were expanded and selected
506 for antibiotic resistance for three weeks. FP-positive cells were selected using FACS and
507 sorted into single cells per well in 96-well plates and clones were expanded and tested for

508 FP presence by amplifying and sequencing the C-terminus of the RELA and PCNA genes
509 from genomic DNA, in order to confirm the presence of the linker and eGFP or mScarlet
510 DNA.

511 *Cell seeding and treatment for fixed image analysis*

512 Cells were seeded at a density of 1,000 cells per well in 384-well plates unless otherwise
513 specified.

514 For comparison of cell shape and cytoskeletal features in the five PDAC cell lines, cells were
515 fixed 2 days after seeding, including 1 hr TNFα treatment. The experiment was carried out
516 with three times (biological replicates) in total, each with four technical replicates (wells) per
517 condition.

518 *TNFα treatment*

519 Cells were treated with human recombinant TNFα diluted in complete medium at a final
520 concentration of 0.1 ng/ml, or 1 ng/ml and 10 ng/ml when specified. TNFα sourced from Sino
521 Biological was diluted in water and used to treat the panel of PDAC lines for Bayesian
522 analysis (Figure 2). Due to lack of availability, TNFα was sourced from R&D Systems and
523 diluted in 0.1% BSA/PBS for all other experiments.

524 *Immunofluorescence*

525 Cells were fixed with warm formaldehyde (FA) dissolved in PBS at a final concentration of
526 4% for 15 min at 37°C then washed three times with PBS. Cells were permeabilised in 0.2%
527 TritonX-100 (Sigma Aldrich) dissolved in PBS for 10 min and blocked in 2% BSA/PBS for 1
528 hr at RT (room temperature). Cells were stained with 10μg/ml Hoechst (Sigma Aldrich) in
529 PBS (1:1,000) for 15 minutes, washed three times and left in PBS/azide before imaging.

530 Cells were incubated with primary antibodies for 2 hr at RT or overnight at 4 °C, washed
531 three times with PBS, and incubated with secondary antibodies for 90 min at RT.

532 Primary antibodies used were rabbit anti-p65/RELA NF-κB (Abcam #16502; 1:500), rat anti-
533 α-tubulin (Bio-Rad #MCA78G; 1:1000), and rabbit anti-pFAK Tyr397 (Invitrogen #44-624G;
534 1:250).

535 Cells were incubated with secondary antibodies for 90 min at RT. Secondary antibodies used
536 were Alexa 647 goat anti-rat IgG (Invitrogen #A21247), Alexa 488 goat anti-rabbit IgG
537 (Invitrogen #A11034), and Alexa 647 goat anti-rabbit IgG (Invitrogen #A21246).

538 For F-actin staining, cells were incubated with Alexa-568 phalloidin (Invitrogen #A12380;
539 1:1000) for 90 min simultaneously with secondary antibodies.

540 *Imaging and automated analysis of fixed cells*

541 A minimum of 21 fields of view per well were imaged using the PerkinElmer Opera confocal
542 microscope using a 20x air objective. Image analysis was performed using custom image
543 analysis scripts created and executed on PerkinElmer's Columbus 2.6.0 software platform.
544 Scripts detected and segmented individual nuclei using Hoechst and the cytoplasm using
545 Tubulin, or RELA when Tubulin is not included in the staining set. Cells touching the image
546 border are filtered out and neighbour contact (% cell border touching another cell) for each
547 remaining cell is calculated. The nuclear region is reduced by 1 px from the nuclear outer
548 border from Hoechst segmentation and the ring region is set as the area 2 px to 6 px outside
549 of the nuclear outer border. Intensities of all stains are calculated in all segmented regions
550 on a single-cell level. A total of 32 geometric, cytoskeletal and Hoechst features were
551 measured in addition to measurements of RELA/RELA-GFP. Texture features were
552 calculated using SER methods with region normalisation. Bright and Spot textures were
553 smoothed to a kernel of 4px to detect large patches (bundles) of actin/tubulin. Ridge texture
554 was non-smoothed to detect sharp ridges (filaments) of actin/tubulin. Elongatedness was
555 calculated as $((2*\text{Cell Length})^2/\text{Cell Area})$. Actin Filament Area was measured using
556 Columbus's 'Find Spots' function applied to the actin channel. Neighbour contact was
557 calculated using an inbuilt Columbus algorithm calculating the percentage of a cell's border

558 in contact with other cell borders. Grouped neighbour contact measurements were
559 generated from non-normalised data rounded to the nearest multiple of ten.

560 *Live cell imaging and analysis*

561 MIA PaCa2 RELA-GFP PCNA-Scarlet and PANC1 RELA-GFP PCNA-Scarlet cells were
562 seeded (1,000 cells/well) in a 384-well plate one day prior to imaging. 4 fields per well were
563 imaged at 10 min intervals with a 20x air objective and an environmental control chamber
564 set to 80% humidity, 5% CO2 and 37°C.

565 For live imaging with TNFα only (no siRNA), cells were imaged for 2 hr prior to and 48 hr
566 following TNFα addition using the Opera QEHS imaging system (PerkinElmer). Nuclear
567 RELA and PCNA intensities were measured using Nuclitrack software (Cooper et al., 2017),
568 with 50-60 cells tracked per treatment, cell line and biological replicate (n = 2). Cells were
569 tracked for 10 hr following TNFα treatment while the total 48 hr imaging period was used to
570 ascertain cell fate (division or death). Each biological replicate consisted of eight technical
571 (well) replicates per cell line and treatment. Missing data points in the center of tracks were
572 imputed using the 'imputeTS' package in R.

573 For live imaging with TNFα and siRNA, cells were imaged for 2 hr prior to and 12 hr following
574 TNFα addition using the Opera Phenix Plus High-Content Screening System (PerkinElmer),
575 with two biological replicates (n = 2). Nuclear RELA was measured in all non-border cells
576 using Harmony software (PerkinElmer). In R, data were smoothed with a Savitzky-Golay
577 filter using the 'Signal' package (filter order p = 1, filter length n = 7).

578 In all experiments, intensity measurements are normalised to the mean of the solvent control
579 measurements (TNFα absence) by cell line, to account for photobleaching and laser power
580 changes. Data with siRNAs are normalised to the non-targeting siRNA controls (solvent
581 control).

582 Nuclear RELA peaks were detected in R as the maximum nuclear RELA intensity by track
583 following Savitzky-Golay filtering using the 'Signal' package (filter order p = 3, filter length n
584 = 11).

585 *GFP-Trap*

586 MIA PaCa2 RELA-GFP cells were cultured in 15 cm dishes to 80 % confluence then treated
587 with TNFα at a final concentration of 0.01 ng/ml, 0.1 ng/ml or 10 ng/ml, or with a solvent
588 control. Co-immunoprecipitation (Co-IP) was carried out using GFP-Trap Agarose beads
589 (Chromotek #gta-10) or with binding control agarose beads (Chromotek #bab-20) using
590 RIPA lysis buffer and according to the manufacturer's protocol. Samples were analysed
591 using mass spectrometry by the ICR proteomics core (Theodoros I Roumeliotis and Jyoti
592 Choudhary).

593 *Cytoskeletal Drug Treatments*

594 2,000 MIA PaCa2 RELA-GFP cells/well were seeded in 384-well plates and treated the next
595 day with the following drugs for 24 hr without TNFα at the specified dose ranges: Paclitaxel
596 (6.25-200 nM; Sigma), Vinblastine (3.125-100 nM; Sigma), Nocodazole (12.5-400 nM;
597 Sigma), Demecolcine (6.25-200 nM; Sigma), Cytochalasin D (0.125-4 μM; Sigma), CK666
598 (12.5-400 μM; Sigma), H1152 (1.25-40 μM; Tocris), Blebbistatin (1.25-40 μM; Sigma),
599 PF573228 (0.625-20 μM; Tocris), and Defactinib (0.625-20 μM; Selleckchem). Cells were
600 treated with SMIFH2 (3.125-100 μM; Abcam) for only 3 hr due to reported cycles of de- and
601 re-polymerisation of 4-8 hr and inefficacy after 16 hr (Isogai et al., 2015). Ranges were
602 selected according to literature and manufacturers' recommendations. Doses for further
603 analysis were selected based on the observed effect on the cytoskeletal target and cell
604 morphology.

605 MIA PaCa2 and PANC1 RELA-GFP cells were seeded at 2,000 cells/well in 384-well plates
606 and treated the following day with selected doses of the small-molecule inhibitors for 2 hr

607 plus additional 1 hr co-incubation with 10 ng/ml TNFα (or DMEM control) prior to fixation. n
608 = 3 biological replicates. Cell feature measurements were calculated as fold changes to
609 controls (DMSO and BSA/PBS) then Z-scored across TNFα treatments and cytoskeletal
610 drugs by cell line. Nuclear RELA measurements were normalised to the mean of all
611 measurements by cell feature across all TNFα treatments by cell line.

612 *Quantification and Statistical Analysis*

613 To analyse cell-to-cell differences in the 35 geometric, cytoskeletal and Hoechst features
614 within and between PDAC cell lines, single cell and well (mean) data were collated from all
615 cell lines and treatments (TNFα 0, 0.01, 0.1 and 10 ng/ml) from three biological replicates.
616 Features were normalised to the mean across all treatments and cell lines for each biological
617 replicate. Features were reduced for Bayesian analysis by clustering normalised single cell
618 measurements into ten clusters using the 'ComplexHeatmap' package in R (Gu et al., 2016),
619 clustering by the Pearson coefficient with complete linkage, as shown in Figure 2 – Figure
620 supplement 1B. Bayesian network models and arc strengths were generated in R using
621 normalised single cell data for the ten reduced features via the 'bnlearn' R package (rsmax2
622 method) (Scutari, 2010). This algorithm depicts unidirectional arcs, so reverse relationships
623 can exist but are not as statistically likely as the directional relationships indicated. Bayesian
624 modelling with cytoskeletal perturbation used data collated from all small molecules and
625 TNFα doses (0, 0.01, 0.1 and 10 ng/ml) for MIA PaCa2 and PANC1 cells.

626 Z-scores in Figure 2 – Figure supplement 2 were calculated per technical replicate using the
627 mean and standard deviation for control measurements for each feature across all lines for
628 each biological replicate (N = 3). Mean Z-scores per feature and cell line were calculated by
629 averaging Z-scores for technical replicates across all biological replicates.

630 Statistical tests were carried out using the 'Rstatix' package and visualised using the 'ggpubr'
631 package in R. Principal Component Analysis (PCA) was carried out in R using the inbuilt

632 ‘prcomp’ function using Z-score data. Graphs were generated in R using the ‘ggplot’ package

633 (Wickham, 2016).

Data Availability

All data generated for this study have been included as source data files.

636 # References

637 Ashall, L., Horton, C.A., Nelson, D.E., Paszek, P., Harper, C.V., Sillitoe, K., Ryan, S., Spiller,
638 D.G., Unitt, J.F., Broomhead, D.S., Kell, D.B., Rand, D.A., Sée, V., White, M.R.H., 2009.
639 Pulsatile stimulation determines timing and specificity of NF-κB-dependent transcription.
640 Science 324, 242–246. https://doi.org/10.1126/science.1164860

641 Baeuerle, P.A., Baltimore, D., 1988. Activation of DNA-binding activity in an apparently
642 cytoplasmic precursor of the NF-kappa B transcription factor. Cell 53, 211–217.
643 https://doi.org/10.1016/0092-8674(88)90382-0

644 Barr, A.R., Cooper, S., Heldt, F.S., Butera, F., Stoy, H., Mansfeld, J., Novák, B., Bakal, C.,
645 2017. DNA damage during S-phase mediates the proliferation-quiescence decision in the
646 subsequent G1 via p21 expression. Nat. Commun. 8, 1–17.
647 https://doi.org/10.1038/ncomms14728

648 Bengtsson, A., Andersson, R., Ansari, D., 2020. The actual 5-year survivors of pancreatic
649 ductal adenocarcinoma based on real-world data. Sci. Rep. 10, 16425.
650 https://doi.org/10.1038/s41598-020-73525-y

651 Bold, R.J., Virudachalam, S., McConkey, D.J., 2001. Chemosensitization of Pancreatic
652 Cancer by Inhibition of the 26S Proteasome. J. Surg. Res. 100, 11–17.
653 https://doi.org/10.1006/jsre.2001.6194

654 Bourgarel-Rey, V., Vallee, S., Rimet, O., Champion, S., Braguer, D., Desobry, A., Briand,
655 C., Barra, Y., 2001. Involvement of nuclear factor kappaB in c-Myc induction by tubulin
656 polymerization inhibitors. Mol. Pharmacol. 59, 1165–1170.
657 https://doi.org/10.1124/mol.59.5.1165

658 Bren, G.D., Solan, N.J., Miyoshi, H., Pennington, K.N., Pobst, L.J., Paya, C.V., 2001.
659 Transcription of the RelB gene is regulated by NF-kappaB. Oncogene 20, 7722–7733.
660 https://doi.org/10.1038/sj.onc.1204868

661 Brown, K., Park, S., Kanno, T., Franzoso, G., Siebenlist, U., 1993. Mutual regulation of the
662 transcriptional activator NF-kappa B and its inhibitor, I kappa B-alpha. Proc. Natl. Acad. Sci.
663 U. S. A. 90, 2532–2536. https://doi.org/10.1073/pnas.90.6.2532

664 Chen, Z., Hagler, J., Palombella, V.J., Melandri, F., Scherer, D., Ballard, D., Maniatis, T.,
665 1995. Signal-induced site-specific phosphorylation targets I kappa B alpha to the ubiquitin-
666 proteasome pathway. Genes Dev. 9, 1586–1597. https://doi.org/10.1101/gad.9.13.1586

667 Collart, M.A., Baeuerle, P., Vassalli, P., 1990. Regulation of tumor necrosis factor alpha
668 transcription in macrophages: involvement of four kappa B-like motifs and of constitutive and
669 inducible forms of NF-kappa B. Mol. Cell. Biol. 10, 1498–1506.
670 https://doi.org/10.1128/mcb.10.4.1498-1506.1990

671 Deer, E.L., Gonzalez-Hernandez, J., Coursen, J.D., Shea, J.E., Ngatia, J., Scaife, C.L.,
672 Firpo, M.A., Mulvihill, S.J., 2010. Phenotype and Genotype of Pancreatic Cancer Cell Lines.
673 Pancreas 39, 425–435. https://doi.org/10.1097/MPA.0b013e3181c15963

674 DiDonato, J.A., Hayakawa, M., Rothwarf, D.M., Zandi, E., Karin, M., 1997. A cytokine-
675 responsive IκB kinase that activates the transcription factor NF-κB. Nature 388, 548–554.
676 https://doi.org/10.1038/41493

677 Frasor, J., Weaver, A., Pradhan, M., Dai, Y., Miller, L.D., Lin, C.-Y., Stanculescu, A., 2009.

Positive cross-talk between estrogen receptor and NF-kappaB in breast cancer. Cancer Res. 69, 8918–8925. https://doi.org/10.1158/0008-5472.CAN-09-2608

Fujioka, S., Sclabas, G.M., Schmidt, C., Frederick, W.A., Dong, Q.G., Abbruzzese, J.L., Evans, D.B., Baker, C., Chiao, P.J., 2003. Function of Nuclear Factor κB in Pancreatic Cancer Metastasis. Clin. Cancer Res. 9, 346–354.

Ghosh, S., May, M.J., Kopp, E.B., 1998. NF-κB and Rel Proteins: Evolutionarily Conserved Mediators of Immune Responses. Annu. Rev. Immunol. 16, 225–260. https://doi.org/10.1146/annurev.immunol.16.1.225

Gigant, B., Wang, C., Ravelli, R.B.G., Roussi, F., Steinmetz, M.O., Curmi, P.A., Sobel, A., Knossow, M., 2005. Structural basis for the regulation of tubulin by vinblastine. Nature 435, 519–522. https://doi.org/10.1038/nature03566

Hayden, M.S., West, A.P., Ghosh, S., 2006. NF-κB and the immune response. Oncogene 25, 6758–6780. https://doi.org/10.1038/sj.onc.1209943

Heid, I., Lubeseder-Martellato, C., Sipos, B., Mazur, P.K., Lesina, M., Schmid, R.M., Siveke, J.T., 2011. Early requirement of Rac1 in a mouse model of pancreatic cancer. Gastroenterology 141, 719–730, 730.e1–7. https://doi.org/10.1053/j.gastro.2011.04.043

Hoffmann, A., Levchenko, A., Scott, M.L., Baltimore, D., 2002. The IκB-NF-κB Signaling Module: Temporal Control and Selective Gene Activation. Science 298, 1241–1245. https://doi.org/10.1126/science.1071914

Isogai, T., van der Kammen, R., Innocenti, M., 2015. SMIFH2 has effects on Formins and p53 that perturb the cell cytoskeleton. Sci. Rep. 5, 9802. https://doi.org/10.1038/srep09802

Kieran, M., Blank, V., Logeat, F., Vandekerckhove, J., Lottspeich, F., Le Bail, O., Urban, M.B., Kourilsky, P., Baeuerle, P.A., Israël, A., 1990. The DNA binding subunit of NF-kappa B is identical to factor KBF1 and homologous to the rel oncogene product. Cell 62, 1007–1018. https://doi.org/10.1016/0092-8674(90)90275-j

Kovács, M., Tóth, J., Hetényi, C., Málnási-Csizmadia, A., Sellers, J.R., 2004. Mechanism of Blebbistatin Inhibition of Myosin II. J. Biol. Chem. 279, 35557–35563. https://doi.org/10.1074/jbc.M405319200

Kunnumakkara, A.B., Guha, S., Krishnan, S., Diagaradjane, P., Gelovani, J., Aggarwal, B.B., 2007. Curcumin Potentiates Antitumor Activity of Gemcitabine in an Orthotopic Model of Pancreatic Cancer through Suppression of Proliferation, Angiogenesis, and Inhibition of Nuclear Factor-κB–Regulated Gene Products. Cancer Res. 67, 3853–3861. https://doi.org/10.1158/0008-5472.CAN-06-4257

Kurki, P., Vanderlaan, M., Dolbeare, F., Gray, J., Tan, E.M., 1986. Expression of proliferating cell nuclear antigen (PCNA)/cyclin during the cell cycle. Exp. Cell Res. 166, 209–219. https://doi.org/10.1016/0014-4827(86)90520-3

Lamarche-Vane, N., Hall, A., 1998. CdGAP, a novel proline-rich GTPase-activating protein for Cdc42 and Rac. J. Biol. Chem. 273, 29172–29177. https://doi.org/10.1074/jbc.273.44.29172

Lamba, V., Ghosh, I., 2012. New directions in targeting protein kinases: focusing upon true allosteric and bivalent inhibitors. Curr. Pharm. Des. 18, 2936–2945. https://doi.org/10.2174/138161212800672813

Lane, K., Valen, D.V., DeFelice, M.M., Macklin, D.N., Kudo, T., Jaimovich, A., Carr, A., Meyer, T., Pe'er, D., Boutet, S.C., Covert, M.W., 2017. Measuring Signaling and RNA-Seq

722 in the Same Cell Links Gene Expression to Dynamic Patterns of NF-κB Activation. Cell Syst.
723 4, 458-469.e5. https://doi.org/10.1016/j.cels.2017.03.010

724 Libermann, T.A., Baltimore, D., 1990. Activation of interleukin-6 gene expression through the
725 NF-kappa B transcription factor. Mol. Cell. Biol. 10, 2327–2334.
726 https://doi.org/10.1128/mcb.10.5.2327-2334.1990

727 Lombardi, L., Ciana, P., Cappellini, C., Trecca, D., Guerrini, L., Migliazza, A., Maiolo, A.T.,
728 Neri, A., 1995. Structural and functional characterization of the promoter regions of the
729 NFKB2 gene. Nucleic Acids Res. 23, 2328–2336. https://doi.org/10.1093/nar/23.12.2328

730 Melisi, D., Niu, J., Chang, Z., Xia, Q., Peng, B., Ishiyama, S., Evans, D.B., Chiao, P.J., 2009.
731 Secreted interleukin-1alpha induces a metastatic phenotype in pancreatic cancer by
732 sustaining a constitutive activation of nuclear factor-kappaB. Mol. Cancer Res. MCR 7, 624–
733 633. https://doi.org/10.1158/1541-7786.MCR-08-0201

734 Mullins, R.D., Heuser, J.A., Pollard, T.D., 1998. The interaction of Arp2/3 complex with actin:
735 Nucleation, high affinity pointed end capping, and formation of branching networks of
736 filaments. Proc. Natl. Acad. Sci. 95, 6181–6186. https://doi.org/10.1073/pnas.95.11.6181

737 Nelson, D.E., Ihekwaba, A.E.C., Elliott, M., Johnson, J.R., Gibney, C.A., Foreman, B.E.,
738 Nelson, G., See, V., Horton, C.A., Spiller, D.G., Edwards, S.W., McDowell, H.P., Unitt, J.F.,
739 Sullivan, E., Grimley, R., Benson, N., Broomhead, D., Kell, D.B., White, M.R.H., 2004.
740 Oscillations in NF-κB Signaling Control the Dynamics of Gene Expression. Science 306,
741 704–708. https://doi.org/10.1126/science.1099962

742 Németh, Z.H., Deitch, E.A., Davidson, M.T., Szabó, C., Vizi, E.S., Haskó, G., 2004.
743 Disruption of the actin cytoskeleton results in nuclear factor-kappaB activation and
744 inflammatory mediator production in cultured human intestinal epithelial cells. J. Cell.
745 Physiol. 200, 71–81. https://doi.org/10.1002/jcp.10477

746 Nolan, G.P., Ghosh, S., Liou, H.C., Tempst, P., Baltimore, D., 1991. DNA binding and I kappa
747 B inhibition of the cloned p65 subunit of NF-kappa B, a rel-related polypeptide. Cell 64, 961–
748 969. https://doi.org/10.1016/0092-8674(91)90320-x

749 Pe'er, D., Regev, A., Elidan, G., Friedman, N., 2001. Inferring subnetworks from perturbed
750 expression profiles. Bioinforma. Oxf. Engl. 17 Suppl 1, S215-224.
751 https://doi.org/10.1093/bioinformatics/17.suppl_1.s215

752 Pruyne, D., Evangelista, M., Yang, C., Bi, E., Zigmond, S., Bretscher, A., Boone, C., 2002.
753 Role of formins in actin assembly: nucleation and barbed-end association. Science 297,
754 612–615. https://doi.org/10.1126/science.1072309

755 Razidlo, G.L., Burton, K.M., McNiven, M.A., 2018. Interleukin-6 promotes pancreatic cancer
756 cell migration by rapidly activating the small GTPase CDC42. J. Biol. Chem. 293, 11143–
757 11153. https://doi.org/10.1074/jbc.RA118.003276

758 Rizvi, S.A., Neidt, E.M., Cui, J., Feiger, Z., Skau, C.T., Gardel, M.L., Kozmin, S.A., Kovar,
759 D.R., 2009. Identification and Characterization of a Small Molecule Inhibitor of Formin-
760 Mediated Actin Assembly. Chem. Biol. 16, 1158–1168.
761 https://doi.org/10.1016/j.chembiol.2009.10.006

762 Rosette, C., Karin, M., 1995. Cytoskeletal control of gene expression: depolymerization of
763 microtubules activates NF-kappa B. J. Cell Biol. 128, 1111–1119.

764 Sachs, K., Perez, O., Pe'er, D., Lauffenburger, D.A., Nolan, G.P., 2005. Causal Protein-
765 Signaling Networks Derived from Multiparameter Single-Cell Data. Science 308, 523–529.

https://doi.org/10.1126/science.1105809

Sailem, H.Z., Bakal, C., 2017. Identification of clinically predictive metagenes that encode components of a network coupling cell shape to transcription by image-omics. Genome Res. 27, 196–207. https://doi.org/10.1101/gr.202028.115

Sasaki, Y., Suzuki, M., Hidaka, H., 2002. The novel and specific Rho-kinase inhibitor (S)-(+)-2-methyl-1-[(4-methyl-5-isoquinoline)sulfonyl]-homopiperazine as a probing molecule for Rho-kinase-involved pathway. Pharmacol. Ther. 93, 225–232.

Scott, M.L., Fujita, T., Liou, H.C., Nolan, G.P., Baltimore, D., 1993. The p65 subunit of NF-kappa B regulates I kappa B by two distinct mechanisms. Genes Dev. 7, 1266–1276. https://doi.org/10.1101/gad.7.7a.1266

Scutari, M., Graafland, C.E., Gutierrez, J.M., 2018. Who Learns Better Bayesian Network Structures: Constraint-Based, Score-based or Hybrid Algorithms? Proc. Mach. Learn. Res. 72, 416–427.

Sero, J.E., Sailem, H.Z., Ardy, R.C., Almuttaqi, H., Zhang, T., Bakal, C., 2015. Cell shape and the microenvironment regulate nuclear translocation of NF-κB in breast epithelial and tumor cells. Mol. Syst. Biol. 11. https://doi.org/10.15252/msb.20145644

Spencer, C.M., Faulds, D., 1994. Paclitaxel. Drugs 48, 794–847. https://doi.org/10.2165/00003495-199448050-00009

Stewart-Ornstein, J., Lahav, G., 2016. Dynamics of CDKN1A in Single Cells Defined by an Endogenous Fluorescent Tagging Toolkit. Cell Rep. 14, 1800–1811. https://doi.org/10.1016/j.celrep.2016.01.045

Sun, S.C., Ganchi, P.A., Ballard, D.W., Greene, W.C., 1993. NF-kappa B controls expression of inhibitor I kappa B alpha: evidence for an inducible autoregulatory pathway. Science 259, 1912–1915. https://doi.org/10.1126/science.8096091

Sung, M.-H., Salvatore, L., Lorenzi, R.D., Indrawan, A., Pasparakis, M., Hager, G.L., Bianchi, M.E., Agresti, A., 2009. Sustained Oscillations of NF-κB Produce Distinct Genome Scanning and Gene Expression Profiles. PLOS ONE 4, e7163. https://doi.org/10.1371/journal.pone.0007163

Tangutur, A.D., Kumar, D., Krishna, K.V., Kantevari, S., 2017. Microtubule Targeting Agents as Cancer Chemotherapeutics: An Overview of Molecular Hybrids as Stabilizing and Destabilizing Agents. Curr. Top. Med. Chem. 17, 2523–2537. https://doi.org/10.2174/1568026617666170104145640

Tay, S., Hughey, J.J., Lee, T.K., Lipniacki, T., Quake, S.R., Covert, M.W., 2010. Single-cell NF-κB dynamics reveal digital activation and analog information processing in cells. Nature 466, 267–271. https://doi.org/10.1038/nature09145

Tcherkezian, J., Triki, I., Stenne, R., Danek, E.I., Lamarche-Vane, N., 2006. The human orthologue of CdGAP is a phosphoprotein and a GTPase-activating protein for Cdc42 and Rac1 but not RhoA. Biol. Cell 98, 445–456. https://doi.org/10.1042/BC20050101

Vallenius, T., Vaahtomeri, K., Kovac, B., Osiceanu, A.-M., Viljanen, M., Mäkelä, T.P., 2011. An association between NUAK2 and MRIP reveals a novel mechanism for regulation of actin stress fibers. J. Cell Sci. 124, 384–393. https://doi.org/10.1242/jcs.072660

Vasquez, R.J., Howell, B., Yvon, A.M., Wadsworth, P., Cassimeris, L., 1997. Nanomolar concentrations of nocodazole alter microtubule dynamic instability in vivo and in vitro. Mol. Biol. Cell 8, 973–985. https://doi.org/10.1091/mbc.8.6.973

810 Wang, W., Abbruzzese, J.L., Evans, D.B., Larry, L., Cleary, K.R., Chiao, P.J., 1999. The
811 Nuclear Factor-κB RelA Transcription Factor Is Constitutively Activated in Human Pancreatic
812 Adenocarcinoma Cells. Clin. Cancer Res. 5, 119–127.

813 Weichert, W., Boehm, M., Gekeler, V., Bahra, M., Langrehr, J., Neuhaus, P., Denkert, C.,
814 Imre, G., Weller, C., Hofmann, H.-P., Niesporek, S., Jacob, J., Dietel, M., Scheidereit, C.,
815 Kristiansen, G., 2007. High expression of RelA/p65 is associated with activation of nuclear
816 factor-*κ*B-dependent signaling in pancreatic cancer and marks a patient population with poor
817 prognosis. Br. J. Cancer 97, 523–530. https://doi.org/10.1038/sj.bjc.6603878

818 Yamamoto, H., Takashima, S., Shintani, Y., Yamazaki, S., Seguchi, O., Nakano, A., Higo,
819 S., Kato, H., Liao, Y., Asano, Y., Minamino, T., Matsumura, Y., Takeda, H., Kitakaze, M.,
820 2008. Identification of a novel substrate for TNFalpha-induced kinase NUAK2. Biochem.
821 Biophys. Res. Commun. 365, 541–547. https://doi.org/10.1016/j.bbrc.2007.11.013

822 Yuan, W.-C., Pepe-Mooney, B., Galli, G.G., Dill, M.T., Huang, H.-T., Hao, M., Wang, Y.,
823 Liang, H., Calogero, R.A., Camargo, F.D., 2018. NUAK2 is a critical YAP target in liver
824 cancer. Nat. Commun. 9, 4834. https://doi.org/10.1038/s41467-018-07394-5

825 Zambrano, S., De Toma, I., Piffer, A., Bianchi, M.E., Agresti, A., 2016. NF-κB oscillations
826 translate into functionally related patterns of gene expression. eLife 5.
827 https://doi.org/10.7554/eLife.09100

828 Zandi, E., Rothwarf, D.M., Delhase, M., Hayakawa, M., Karin, M., 1997. The IkappaB kinase
829 complex (IKK) contains two kinase subunits, IKKalpha and IKKbeta, necessary for IkappaB
830 phosphorylation and NF-kappaB activation. Cell 91, 243–252. https://doi.org/10.1016/s0092-
831 8674(00)80406-7

832 Zhao, X., Fan, W., Xu, Z., Chen, H., He, Y., Yang, Gui, Yang, Gang, Hu, H., Tang, S., Wang,
833 P., Zhang, Z., Xu, P., Yu, M., 2016. Inhibiting tumor necrosis factor-alpha diminishes
834 desmoplasia and inflammation to overcome chemoresistance in pancreatic ductal
835 adenocarcinoma. Oncotarget 7, 81110–81122. https://doi.org/10.18632/oncotarget.13212

836 # Figure Titles and Legends

837 **Figure 1: Single cell analysis of live endogenous RELA-GFP dynamics with TNFα in**
838 **human pancreatic cell lines**

839 (A) Schematic of CRISPR gRNA and homology construct with neomycin (neo) resistance for
840 tagging of the RELA C-terminus with GFP. (B) Confocal microscopy images of MIA PaCa2
841 and PANC1 monoclonal cell lines expressing endogenously tagged RELA-GFP and PCNA-
842 Scarlet and treated with 1 hr solvent control or 0.1 ng/ml TNFα. (C) Tracks of single cell
843 nuclear RELA-GFP intensity measurements in MIA PaCa2 and PANC1 cells from -120 min
844 to +600 min relative to TNFα addition (0.01 ng/ml, 0.1 ng/ml and 10 ng/ml) . n = 50-60 tracked
845 cells per TNFα dose for each of two experimental repeats. (D) Amplitude and (E) time of first
846 nuclear RELA-GFP intensity peak in MIA PaCa2 cand PANC1 single cells. Boxplots show
847 median and interquartile range. M = median per cluster. σ = standard deviation.(F) Pearson's
848 correlation coefficient (r) between nuclear RELA-GFP intensity at 60 min versus 180, 300 or
849 600 min within single cell RELA-GFP tracks. Data are normalised within each track to nuclear
850 RELA-GFP intensity at 0 min.

851 **Figure 2: Bayesian network analysis predicts statistical dependence of RELA on actin**

852 (A) Single cell nuclear RELA intensity distributions by immunofluorescence and automated
853 image analysis. (B) Schematic depicting generation of a Bayesian network model for
854 probabilistic relationships between cell features in PDAC cells. PDAC cells were treated with
855 0, 0.01, 0.1 or 10 ng/ml TNFα for 1 hr. Using automated image analysis of cell markers,
856 features are measured on a single cell basis and Bayesian analysis is used to detect linear
857 and non-linear relationships between the features. These relationships are then incorporated
858 into a Bayesian network model, which is an influence diagram consisting of nodes, each
859 representing a measured feature, and arcs between the nodes that depict predicted
860 dependencies between the nodes. (C) Bayesian network model incorporating data from all

861 PDAC lines treated for 1 hr with 0 (solvent control), 0.01, 0.1 or 10 ng/ml TNFα. Values next
862 to arcs represent the strength of the probabilistic relationship expressed by the arc (arc
863 strength). Orange arcs connect features predicted to depend on nuclear RELA mean, and
864 orange arcs connect features predicted to influence nuclear RELA mean. (D) Dependencies
865 involving nuclear RELA mean in Bayesian network models generated with single cell data
866 for individual treatments or cell lines, or for all cell lines collated (top row in each cell feature
867 section), or all treatments collated (rightmost column in each cell feature section). Purple
868 indicates that nuclear RELA mean is predicted to depend on the cell feature in the Bayesian
869 network model. Orange represents that a cell feature is predicted to depend on nuclear RELA
870 intensity. Dependency strengths are calculated as $\log_2(|\text{arc strength}|)$, multiplied by -1 for
871 dependencies of cell features on nuclear RELA intensity. (E) Schematic indicating small
872 molecules targeting the cytoskeleton. CK666 inhibits the ARP2/3 complex that mediates
873 actin filament nucleation and branching (Mullins et al., 1998). SMIFH2 inhibits formins (Rizvi
874 et al., 2009), which produce long straight filaments by promoting actin nucleation and
875 filament elongation (Pruyne et al., 2002). Cytochalasin D binds to the growing end of actin
876 filaments and inhibits polymerisation (Schliwa, 1982). H1152 targets Rho-kinase (ROCK),
877 preventing ROCK phosphorylation of myosin light chain that normally promotes actin-binding
878 and contractility, while blebbistatin blocks myosin II ATPase and actin contractility (Sasaki et
879 al., 2002; Kovács et al., 2004). Tubulin-targeting drugs prevent MT assembly (vinblastine
880 and nocodazole), limit MT formation and cause MT depolymerisation (demecolcine), or
881 stabilise MTs and prevent disassembly (paclitaxel) (Spencer and Faulds, 1994; Vasquez et
882 al., 1997; Gigant et al., 2005). Focal adhesion kinase (FAK) regulates turnover of focal
883 adhesions, which are integrin-containing complexes linking intracellular actin to extracellular
884 substrates. (F) Bayesian network model generated by single cell data from MIA PaCa2 and
885 PANC1 cells treated separately with the small molecules in (E) for 3 hr then treated with
886 TNFα (0, 0.01, 0.1 or 10 ng/ml) for 1 hr. Numbers indicate arcs strengths. In the presence of
887 small molecule inhibition of the cytoskeleton, nuclear RELA mean is predicted to be

888 dependent on cytoplasm actin mean alone (indicated by the purple arc connecting
889 'cytoplasm actin mean' and 'nuc RELA mean').

890 **Figure 3: RNA-seq analysis of genes regulated by TNFα and RELA in human PDAC**
891 **cells**

892 (A) Volcano plot of p-value against mean fold-change (log2) per gene comparing RNA
893 expression with high TNFα (0.1 ng/ml or 10 ng/ml) to control conditions (no TNFα) across
894 MIA PaCa2 and PANC1 cells. Counts were normalised and log2 fold-changes were
895 calculated using DESeq2. (B) Mean fold-change (log2) across in MIA PaCa2 and PANC1
896 cells for genes significantly downregulated (n = 68) or upregulated (n = 186) by TNFα ($p <$
897 0.01) from (A). Also displayed are the maximum, median and minimum absolute fold
898 changes for downregulated and upregulated genes. (C) Clustered heatmap of TNFα
899 regulated genes. Normalised counts from DESeq2 were log2 transformed and relative to the
900 respective control (no TNFα or IκB-SR) per timepoint (1 hr or 5 hr) and cell line (MIA PaCa2
901 or PANC1), then z-scored across all samples independent per gene. Columns are annotated
902 by gene and rows are annotated by cell line, TNFα dose and time, and presence of IκB-SR.
903 (D) Z-scores for all genes per cluster, faceted by cell line and treatment time (1 hr or 5 hr).
904 Ribbons show the 95 % confidence interval and the middle line depicts the mean. Colour
905 corresponds to presence of IκB-SR. (D') Individual genes within Cluster 3, coloured by gene
906 for control (no IκB-SR) data and grey for all data with IκB-SR (all genes).

907 **Figure 4: Effect of siRNA knockdown of TNFα and actin signalling on RELA dynamics**

908 (A) Tracks of RELA-GFP intensity measurements relative to 10 ng/ml TNFα addition (-2 hr
909 to +12 hr) in MIA PaCa2 and PANC1 cells following 48 hr siRNA incubation. Data show well
910 means from two experimental repeats. Grey lines represent RELA-GFP measurements with
911 non-targeting (NT) siRNA and are identical in all facets. Orange lines show RELA-GFP tracks
912 from cells with siRNA depletion for the target gene indicated in the column facet. (B) Nuclear
913 RELA-GFP intensity measurements (well means from two experimental repeats) for data in

914 at 1 hr (left graph) or 12 hr (right graph) following 10 ng/ml TNFα addition. Statistical results
915 are shown for multiple t-tests with Benjamini-Hochberg correction comparing measurements
916 from each siRNA to the non-targeting siRNA control, independently by cell line and treatment
917 (0 or 10 ng/ml TNFα). All data are normalised to the mean nuclear RELA intensity of the non-
918 targeting control by experimental repeat (n = 2) and cell line. Blue boxplots represent
919 statistically significant ($p < 0.05$) results and grey boxplots show statistically non-significant
920 results ($p <$ value). (C) Snapshots from confocal microscopy timelapse imaging of
921 endogenous RELA-GFP and PCNA-Scarlet (nuclear marker) in MIA PaCa2 and PANC1
922 cells following NT, ARHGAP31 or NUAK2 48 hr siRNA treatment, followed by 1 hr or 12 hr
923 10 ng/ml TNFα addition.

924 **Figure 1 - figure supplement 1: Cell cycle independence of TNFα-mediated RELA**
925 **dynamics in PDAC cells**

926 (A) Confocal microscopy images of PCNA-Scarlet in representative MIA PaCa2 and PANC1
927 nuclei in G1, early S, late S or G2 cell cycle stage. (B) Single cell nuclear RELA-GFP tracks
928 for MIA PaCa2 and PANC1 cells categorised by cell cycle stage at the time of TNFα addition
929 (0.01, 0.1 or 10 ng/ml), based on the intensity and appearance of PCNA-Scarlet. (C) Single
930 cell measurements of nuclear RELA intensity at track peak and (D) time to track peak by cell
931 cycle stage at TNFα addition. (E) Mean nuclear RELA intensity per single cell track, by cell
932 cycle stage at TNFα addition.

933 **Figure 2 - figure supplement 1: Automated image analysis of RELA localisation, cell**
934 **shape, and the cytoskeleton in human cells**

935 (A) Staining by immunofluorescence (α-tubulin and RELA) and dyes marking DNA (Hoechst)
936 and F-actin (phalloidin). Cell regions were segmented using Hoechst and α-Tubulin stains
937 and features were measured in these regions using the four stains. (B) Hierarchical
938 clustering of 35 normalised cell features (excluding RELA measurements) measured in five

939 PDAC cell lines. (C) Selected features (one per cluster) are highlighted in the dendrogram
940 and displayed in the images beside.

941 **Figure 2 - figure supplement 2: Principal components analysis of five human PDAC**
942 **cell lines with a reduced set of cytoskeletal and cell shape features**

943 Principal Component Analysis (PCA) of the ten reduced features used in Bayesian analysis
944 for five PDAC cell lines using two principal components (PC1 and PC2). Overlayed is a biplot
945 (arrows) as an indication of the contribution of each cell feature to the two PCs. Circles
946 represent technical replicates. n = four biological repeats. Horizontal bar graphs for individual
947 cell lines show mean z-scores for each feature, calculated across the six cell lines to
948 compare differences in each feature between the cell lines. Z-scores were calculated using
949 the mean and standard deviation for control measurements across all lines for each
950 biological repeat. Displayed is the mean Z score across all biological repeats (n = 4). Images
951 for each cell line show Hoechst, phalloidin marking F-actin (Actin), α-tubulin (Tubulin) and
952 RELA staining by immunofluorescence.

953 **Figure 2 - figure supplement 3: Dose responses for cytoskeleton-targeting drugs**

954 Dose response curves and representative images of MIA PaCa2 cells treated with small
955 molecules in the absence of TNFα. n = four technical replicates per drug dose. (A & B) 24 hr
956 treatment with tubulin-targeting: vinblastine (0-100 nM), paclitaxel (0-200 nM), nocodazole
957 (0-400 nM) and demelcoline (0-200 nM). (C & E) 24 hr treatment with actin-targeting drugs:
958 cytochalasin D (0-4 μM) and CK666 (0-400 μM). (D & E) 24 hr treatment with myosin-
959 targeting drugs: H1152 (0-40 μM) and blebbistatin (0-40 μM). (F) 3 hr treatment with the
960 actin-targeting drug SMIFH2 (0-100 μM). (G) 24 hr treatment with the FAK inhibitors PF-
961 573228 (PF228; 0-2 μM) and defactinib (0-20 μM).

962 **Figure 3 - figure supplement 1: Hierarchical clustering of TNFα/RELA-regulated gene**
963 **expression in PDAC cells**

964 (A) RNA-seq expression of genes encoding NF-κB (left) and IκB (proteins) in MIA PaCa2
965 and PANC1 cells treated with TNFα for 1 or 5 hr, in the presence of IκB-SR (constitutively
966 active IκB) or a DMSO control. Normalised counts were generated by DESeq2 and $\log_2$
967 transformed. (A'' and A''') Statistical analysis (t-tests with Benjamini-Hochberg correction) of
968 data in (A) comparing RNA expression of each gene (A'') between cells treated with TNFα
969 (data from 0.1 and 10 ng/ml, and 1 hr and 5 hr treatment collated) with the presence or
970 absence of IkB-SR; or (A''') between cells with 1 hr or 5 hr TNFα treatment (0.1 and 10 ng/ml
971 collated) in the absence of IkB-SR. ns (non-significant) = $p > 0.05$, * = $0 < 0.05$, ** = $p < 0.01$.
972 (B) Summary of proteins detected by Co-IP and mass spectrometry using GFP-Trap in MIA
973 PaCa2 RELA-GFP cells. Cells were treated with TNFα (0, 0.01, 0.1 or 10 ng/ml) for 1 hr.
974 Pull-downs were analysed using mass spectrometry. n = 1 experimental repeats for 0 and
975 10 ng/ml TNFα and n = 2 experiments repeats for 0.01 and 0.1 ng/ml TNFα. Protein
976 abundances at each TNFα dose adjusted to RELA abundance.

977 **Figure 4 - figure supplement 1: siRNAs targeting the NF-κB pathway and the NF-κB**
978 **regulated genes *NUAK2* and *ARHGAP31* affect cell morphology and actin**
979 **organisation**

980 Confocal images of mean actin intensity in the cytoplasm of MIA PaCa2 and PANC1 cells
981 transfected with siRNAs for 48 hr: non-targeting (NT); the NF-κB proteins RELA, RELB, and
982 NFKB2; or the NF-κB inhibitors NFKBIA, NFKBIB, and NFKBIE. Cells were stained with
983 phalloidin for F-actin visualisation.

Figure 1

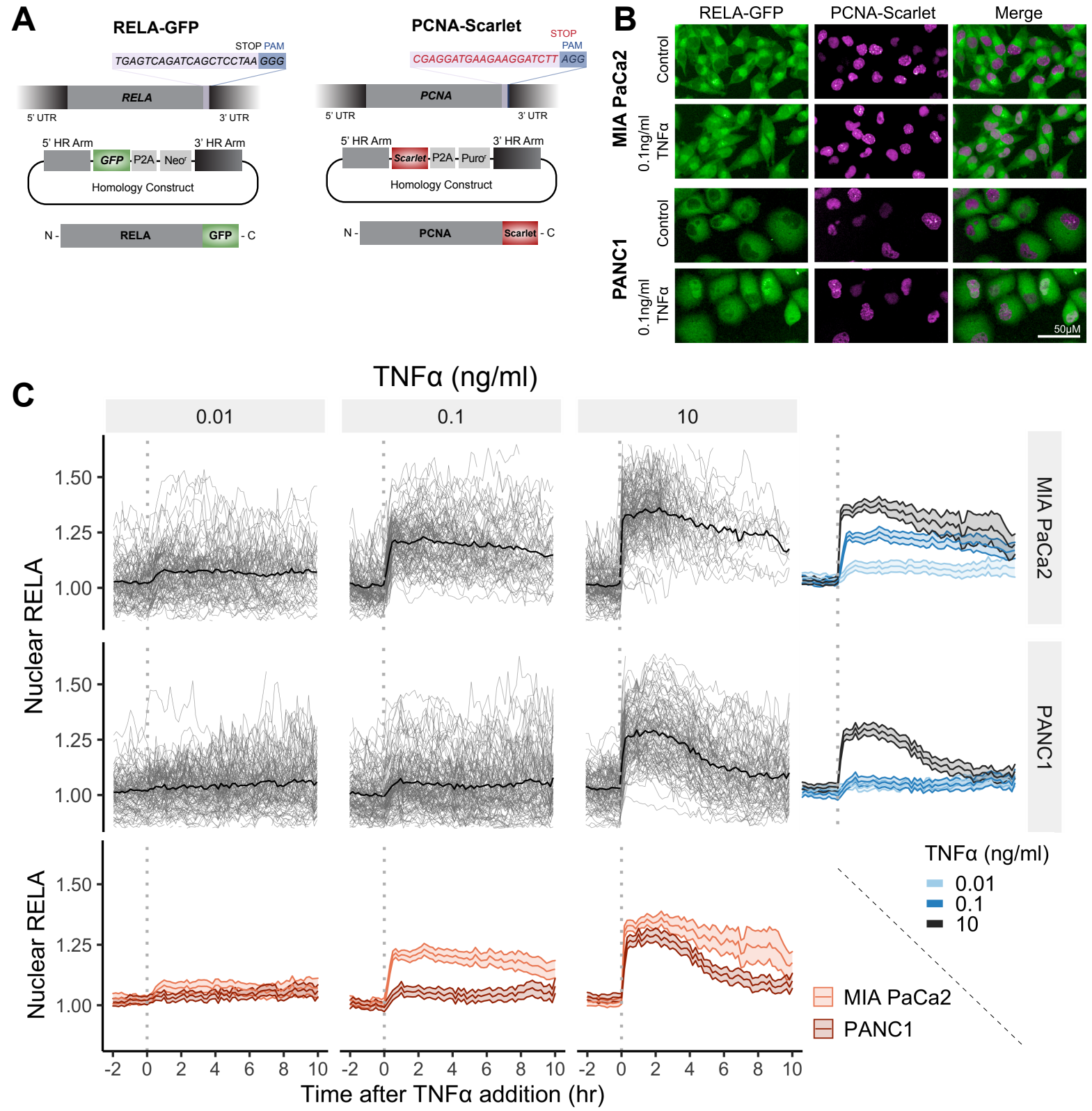
A
RELA-GFP
STOP PAM
TGAGTCAGATCAGCTCCTAA GGG
RELA
5' UTR
3' UTR
5' HR Arm
3' HR Arm
GFP
P2A
Neo
Homology Construct
N - RELA GFP - C
PCNA-Scarlet
STOP
PAM
CGAGGATGAAGAAGGATCTT AGG
PCNA
5' UTR
3' UTR
5' HR Arm
3' HR Arm
Scarlet
P2A
Puro
Homology Construct
N - PCNA Scarlet - C
B
RELA-GFP
PCNA-Scarlet
Merge
MIA PaCa2
Control
0.1ng/ml TNFα
PANC1
Control
0.1ng/ml TNFα
50μM
C
TNFα (ng/ml)
0.01
0.1
10
Nuclear RELA
1.50
1.25
1.00
MIA PaCa2
PANC1
TNFα (ng/ml)
0.01
0.1
10
MIA PaCa2
PANC1
-2 0 2 4 6 8 10
Time after TNFα addition (hr)
D
MIA PaCa2
PANC1
Peak RELA (amplitude)
2.00
1.75
1.50
1.25
1.00
****
ns
Rep
1
2
TNFα log10 (ng/ml)
E
MIA PaCa2
PANC1
Time to peak RELA
200
150
100
50
ns
Rep
1
2
TNFα log10 (ng/ml)
F
MIA PaCa2
PANC1
Correlation (r)
0.8
0.6
0.4
Relative nuc RELA at 60 min vs.
180 min
300 min
600 min
TNFα log10 (ng/ml)

Figure 2

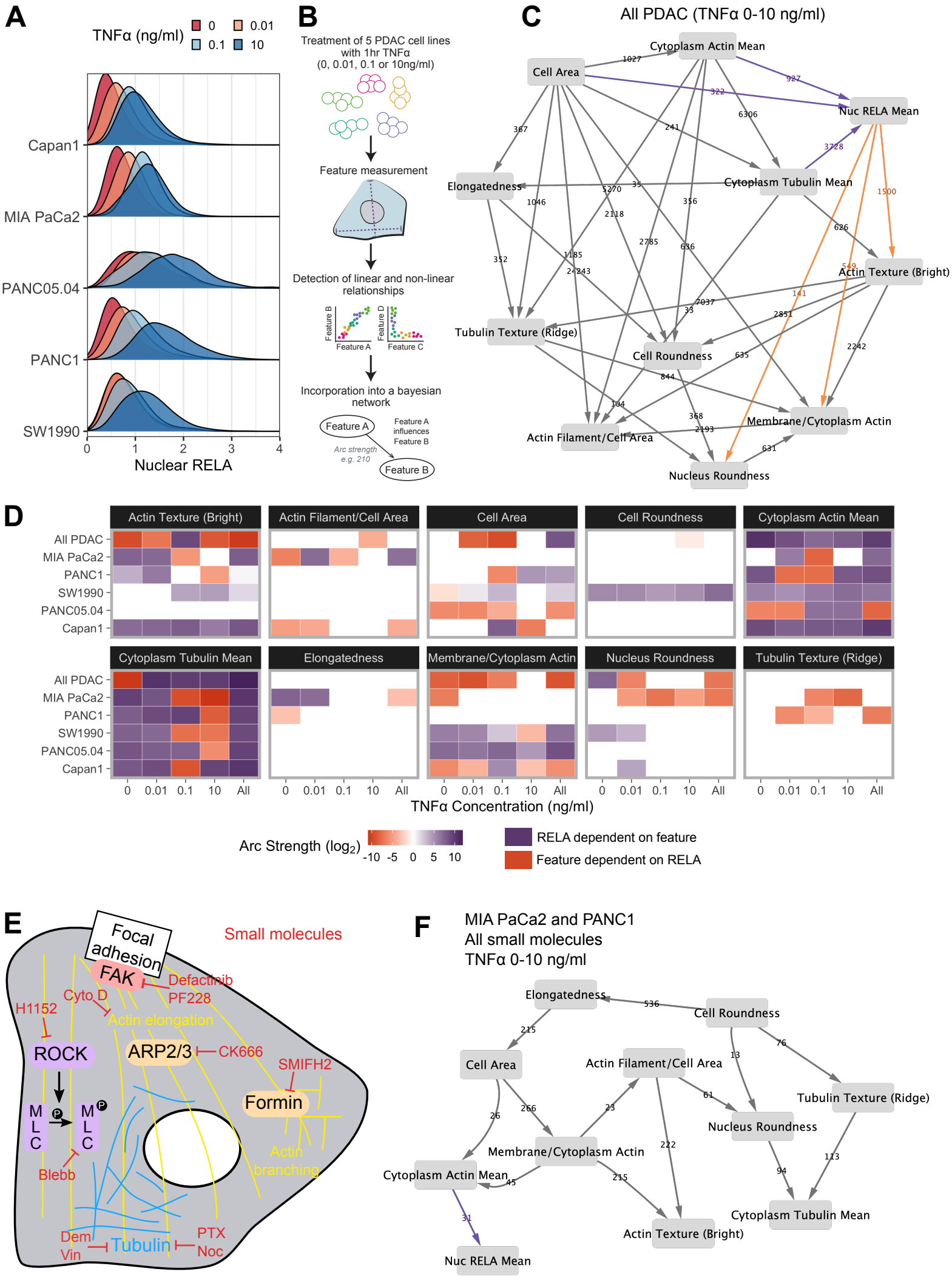
A
TNFα (ng/ml)
0
0.01
0.1
10
Capan1
MIA PaCa2
PANC05.04
PANC1
SW1990
0
1
2
3
4
Nuclear RELA
B
Treatment of 5 PDAC cell lines with 1hr TNFα (0, 0.01, 0.1 or 10ng/ml)
Feature measurement
Detection of linear and non-linear relationships
Feature B
Feature A
Feature D
Feature C
Incorporation into a bayesian network
Feature A
Feature A influences Feature B
Arc strength e.g. 210
Feature B
C
All PDAC (TNFα 0-10 ng/ml)
Cytoplasm Actin Mean
Cell Area
Nuc RELA Mean
Elongatedness
Cytoplasm Tubulin Mean
Actin Texture (Bright)
Tubulin Texture (Ridge)
Cell Roundness
Membrane/Cytoplasm Actin
Actin Filament/Cell Area
Nucleus Roundness
D
Actin Texture (Bright)
Actin Filament/Cell Area
Cell Area
Cell Roundness
Cytoplasm Actin Mean
Cytoplasm Tubulin Mean
Elongatedness
Membrane/Cytoplasm Actin
Nucleus Roundness
Tubulin Texture (Ridge)
All PDAC
MIA PaCa2
PANC1
SW1990
PANC05.04
Capan1
0
0.01
0.1
10
All
TNFα Concentration (ng/ml)
Arc Strength (log2)
-10
-5
0
5
10
RELA dependent on feature
Feature dependent on RELA
E
Focal adhesion
Small molecules
FAK
Defactinib
PF228
Cyto D
H1152
Actin elongation
ROCK
ARP2/3
CK666
SMIFH2
Formin
MLC
P
Blebb
Actin branching
Dem
Vin
Tubulin
PTX
Noc
F
MIA PaCa2 and PANC1
All small molecules
TNFα 0-10 ng/ml
Elongatedness
Cell Roundness
Cell Area
Actin Filament/Cell Area
Tubulin Texture (Ridge)
Nucleus Roundness
Membrane/Cytoplasm Actin
Cytoplasm Actin Mean
Cytoplasm Tubulin Mean
Actin Texture (Bright)
Nuc RELA Mean

Figure 3

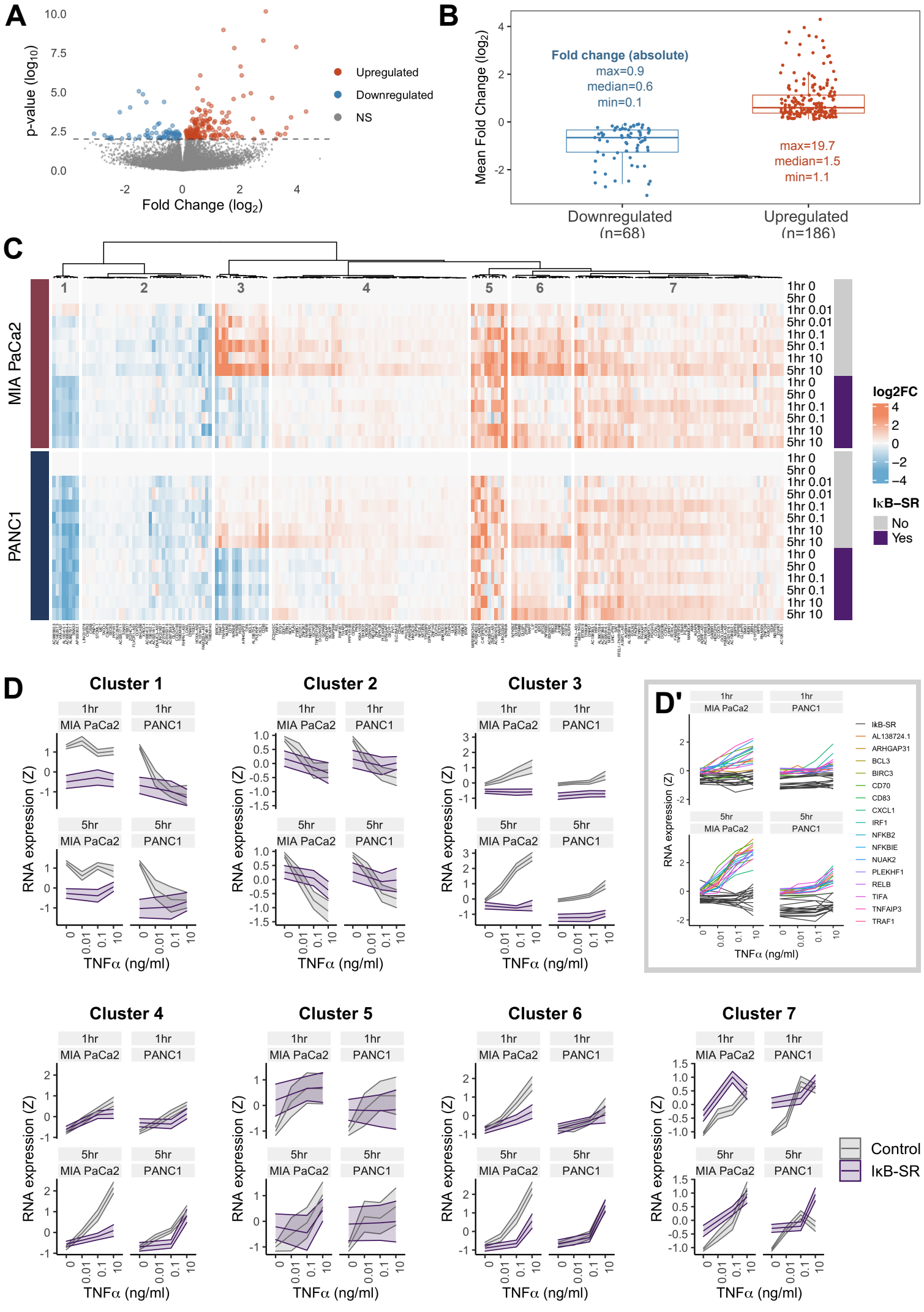
A
p-value (log10)
Fold Change (log2)
Upregulated
Downregulated
NS
B
Mean Fold Change (log2)
Fold change (absolute)
max=0.9
median=0.6
min=0.1
max=19.7
median=1.5
min=1.1
Downregulated (n=68)
Upregulated (n=186)
C
MIA PaCa2
PANC1
log2FC
IκB–SR
No
Yes
D
Cluster 1
Cluster 2
Cluster 3
Cluster 4
Cluster 5
Cluster 6
Cluster 7
RNA expression (Z)
TNFα (ng/ml)
Control
IκB-SR
D'
IκB-SR
AL138724.1
ARHGAP31
BCL3
BIRC3
CD70
CD83
CXCL1
IRF1
NFKB2
NFKBIE
NUAK2
PLEKHF1
RELB
TIFA
TNFAIP3
TRAF1

Figure 4

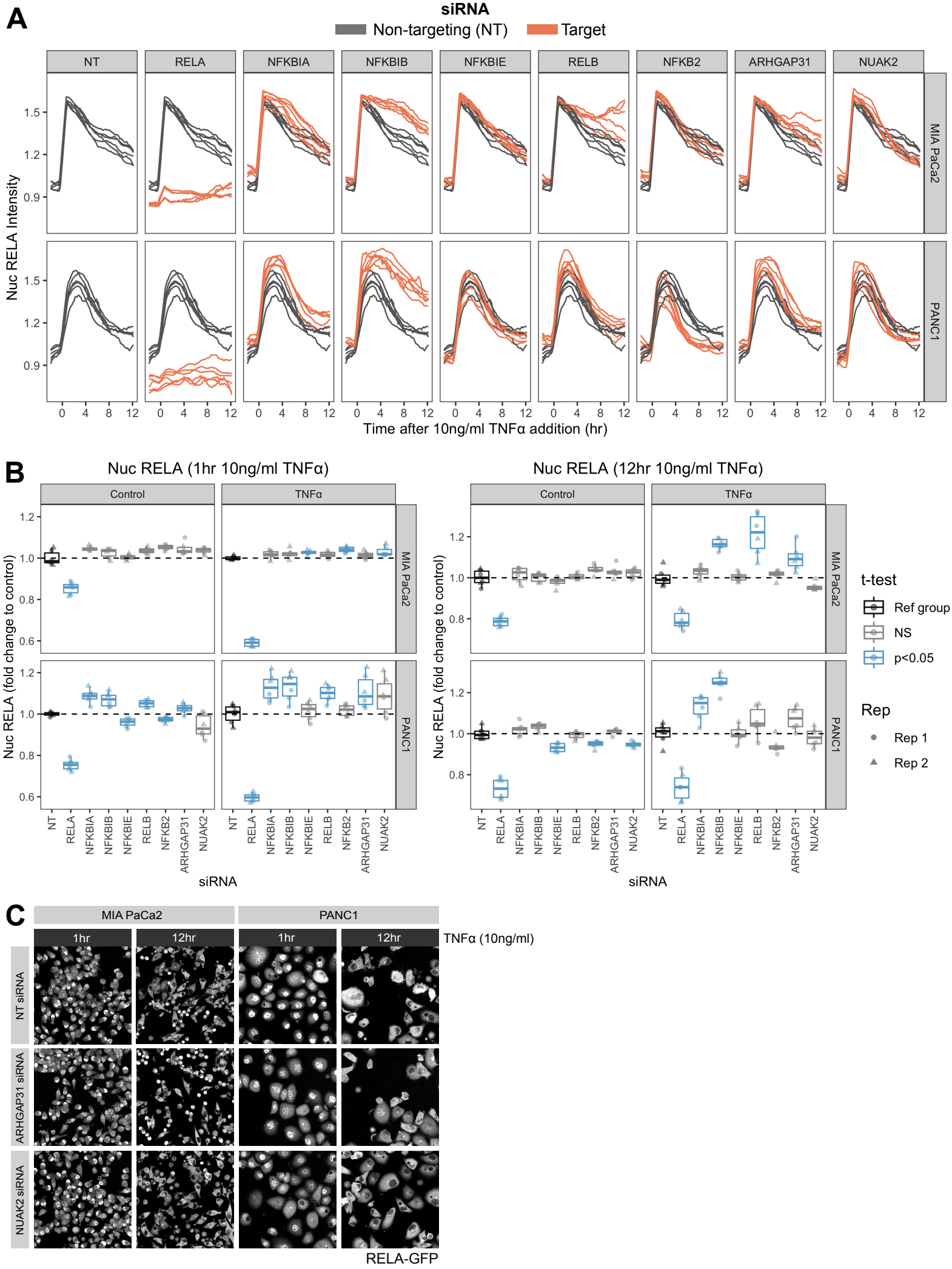
A
siRNA
Non-targeting (NT)
Target
NT
RELA
NFKBIA
NFKBIB
NFKBIE
RELB
NFKB2
ARHGAP31
NUAK2
MIA PaCa2
PANC1
Nuc RELA Intensity
Time after 10ng/ml TNFα addition (hr)
B
Nuc RELA (1hr 10ng/ml TNFα)
Nuc RELA (12hr 10ng/ml TNFα)
Control
TNFα
Nuc RELA (fold change to control)
siRNA
t-test
Ref group
NS
p<0.05
Rep
Rep 1
Rep 2
C
MIA PaCa2
PANC1
1hr
12hr
TNFα (10ng/ml)
NT siRNA
ARHGAP31 siRNA
NUAK2 siRNA
RELA-GFP

Figure 1 - Supplement 1

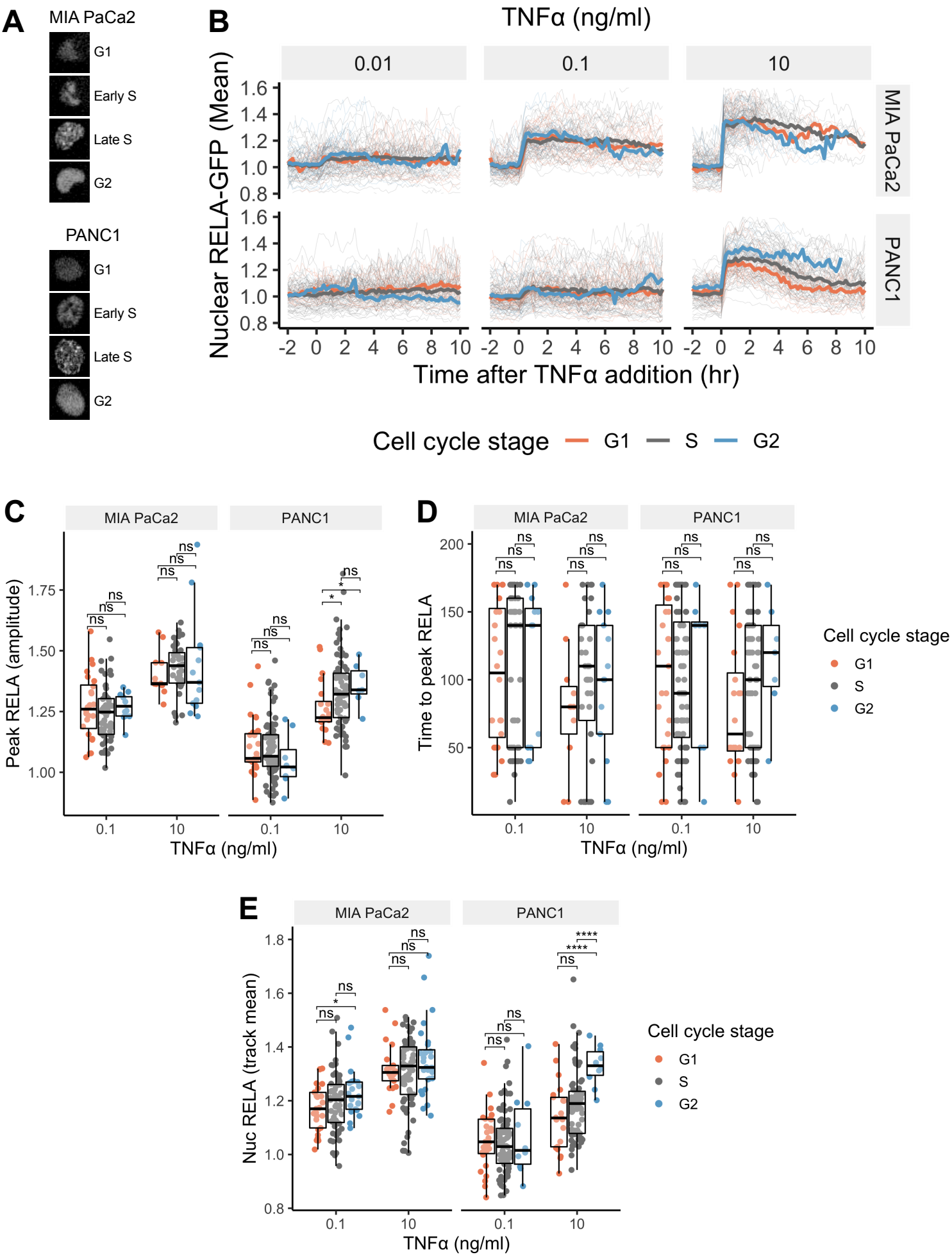

Figure 2 - Supplement 1

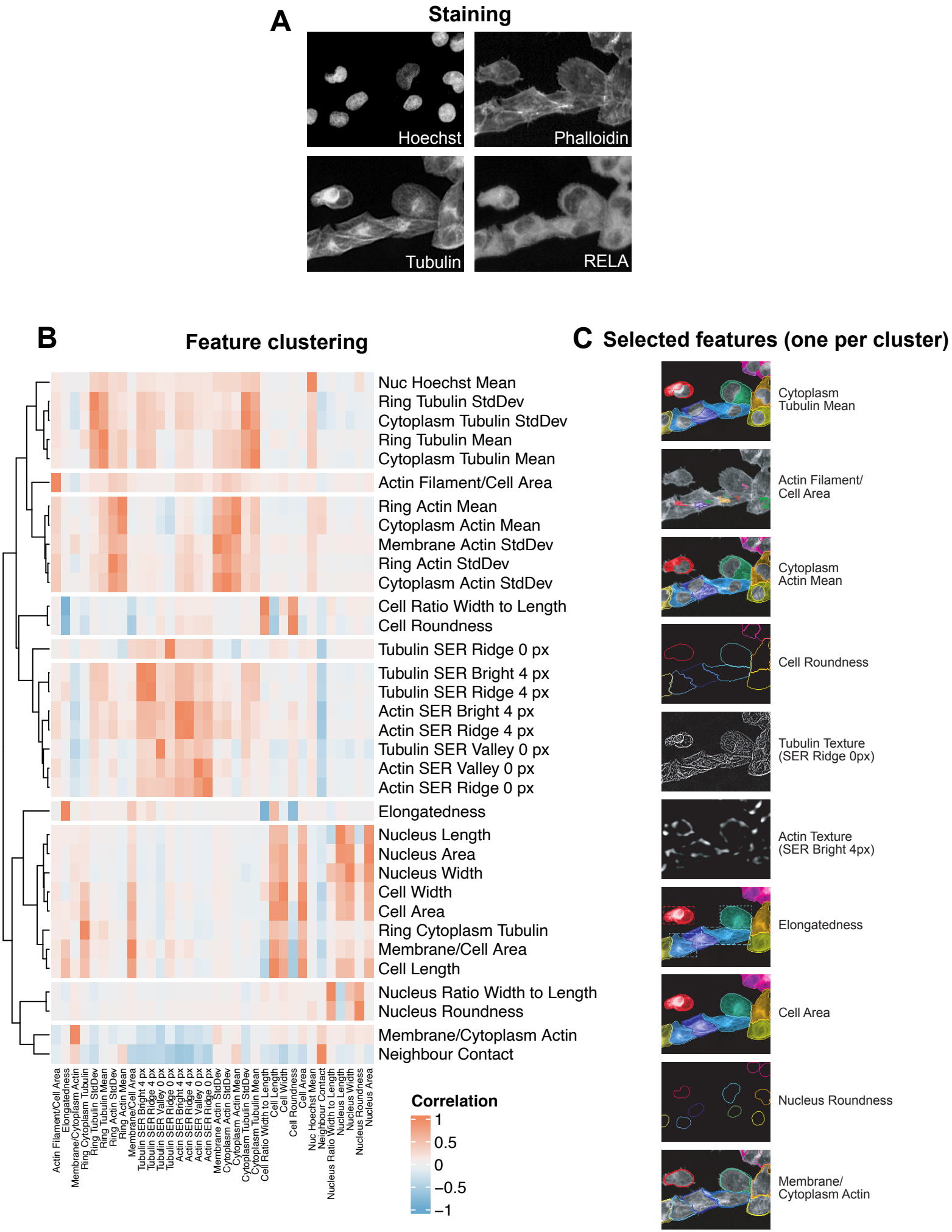

Figure 2 - Supplement 2

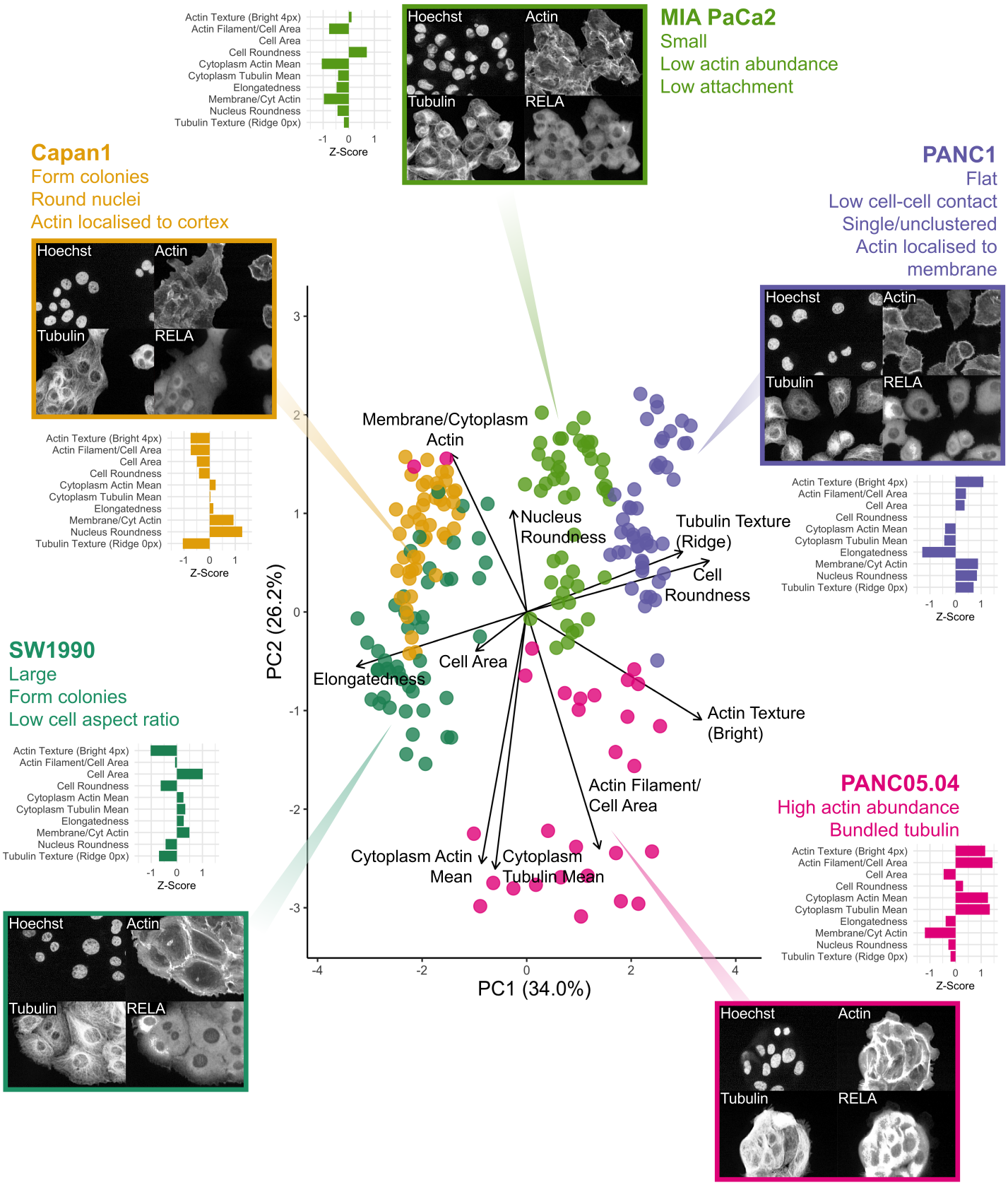

Figure 2 - Supplement 3

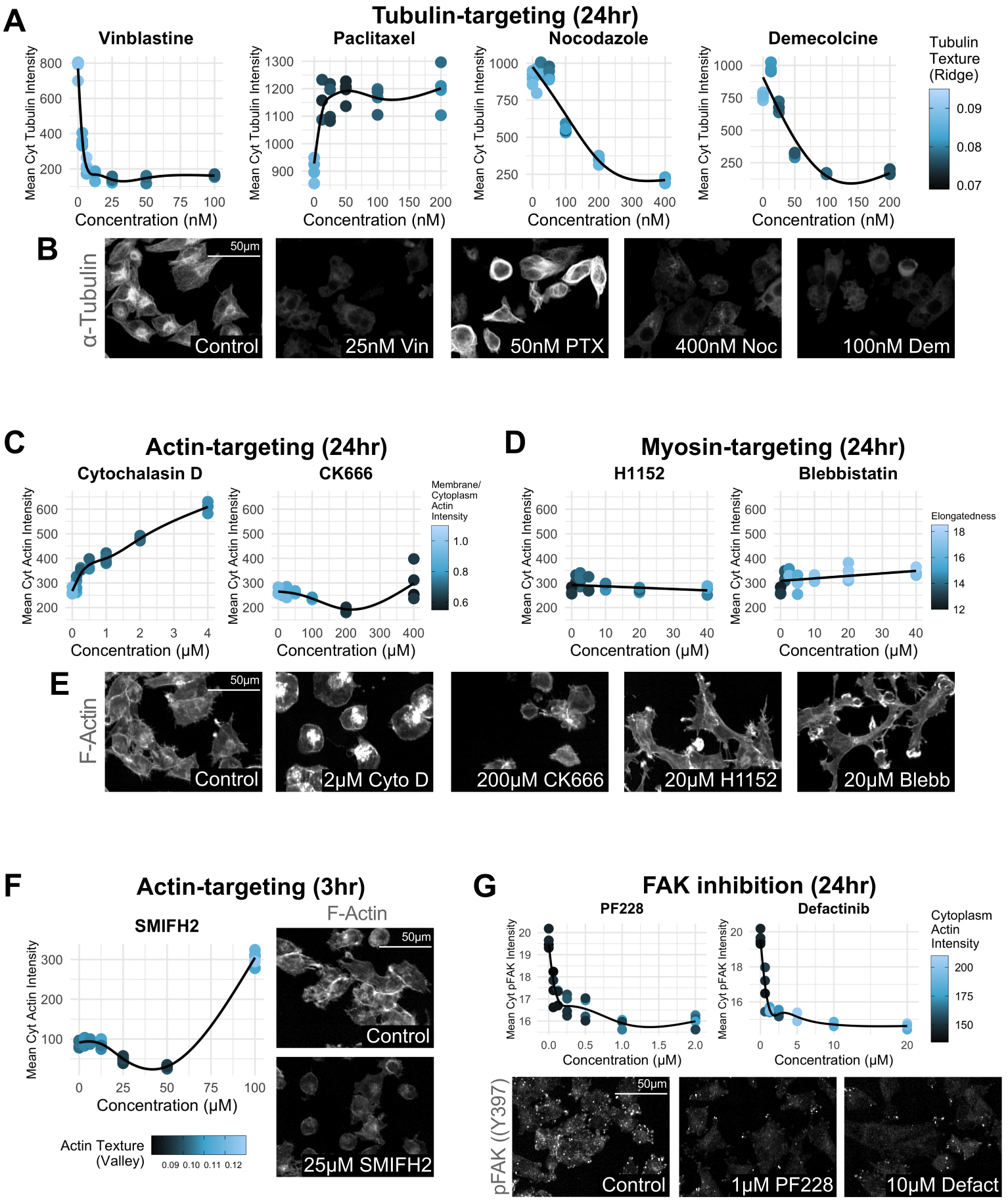

Figure 3 - Supplement 1

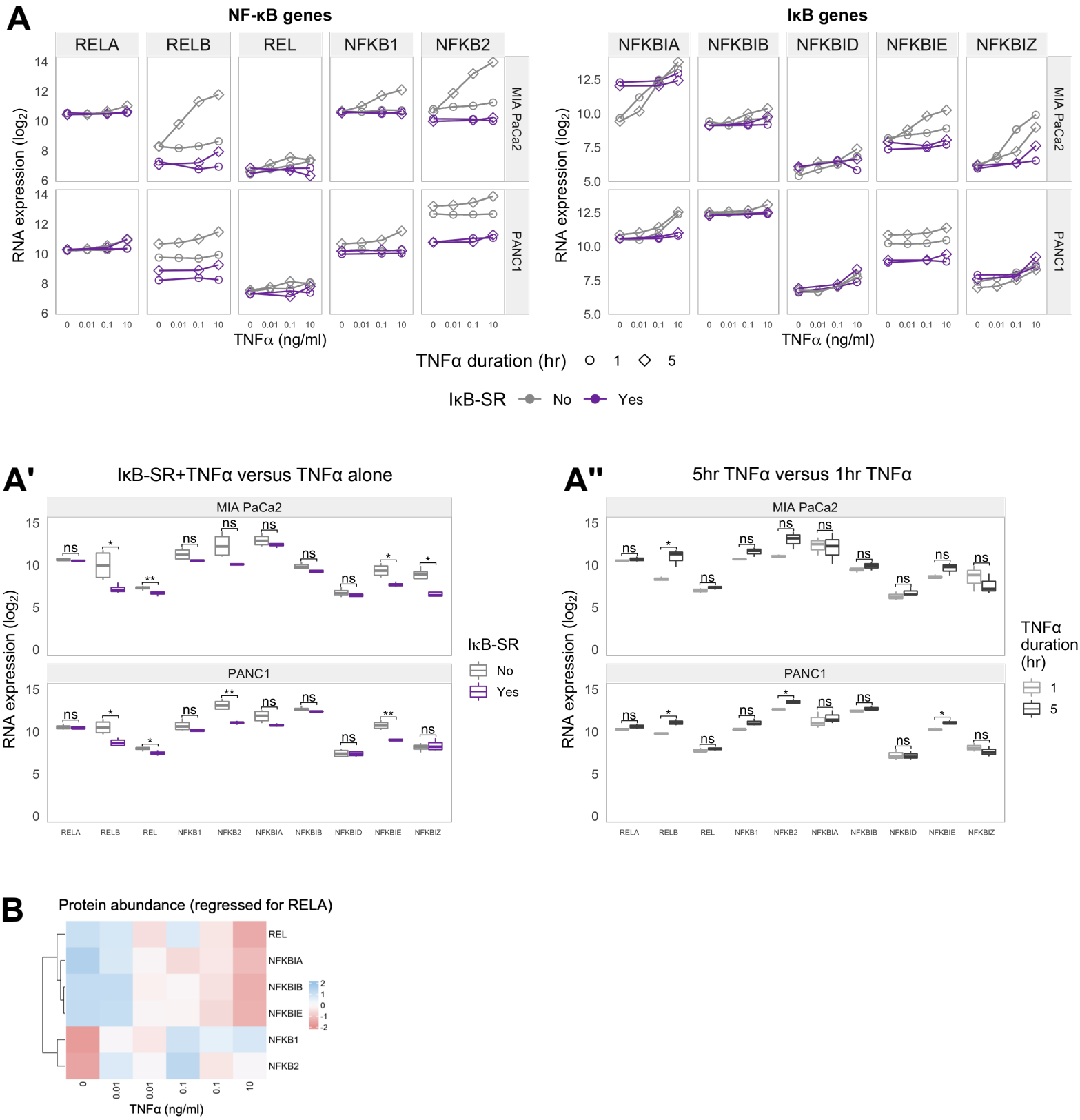
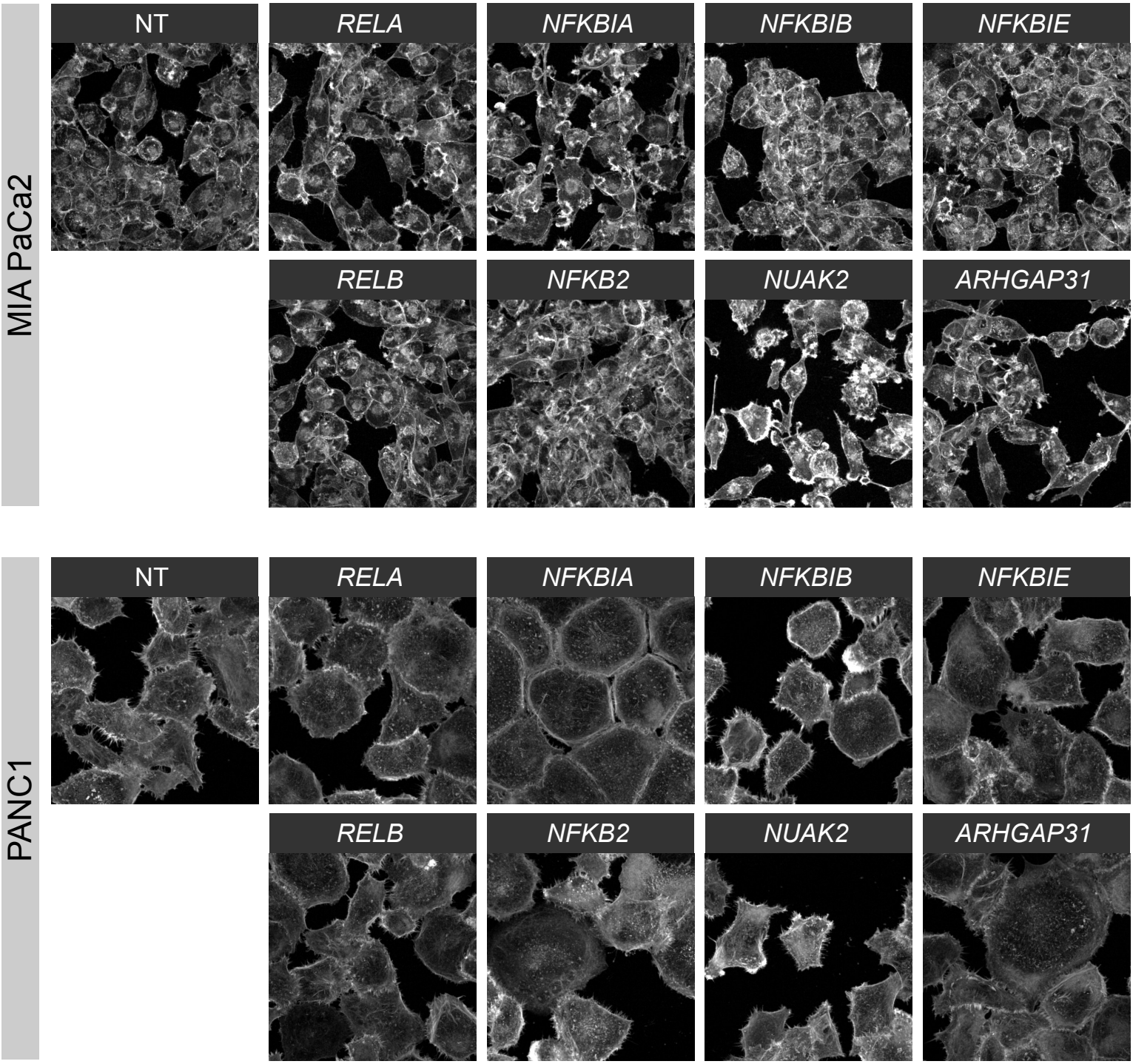
Figure 4 - Supplement 1